UNIVERSITÀ DEGLI STUDI DI MILANO

Department of Clinical Sciences and Community Health

Epidemiology, Epigenetics and Toxicology Laboratory
EPIGET

PhD in:
epidemiology, environmental and public health
Cycle XXX

AIR POLLUTION EXPOSURE AND HEALTH EFFECTS: CELL-SHED MICROVESICLES AS CARRIERS FOR INTERCELLULAR COMMUNICATION

PhD student:

Dott.ssa Roberta Mercorio

Supervisor:

Prof. Angela Cecilia Pesatori

2017-2018

A mio marito Carmine
e al piccolo Gaetano

"Molto ragionamento e poca osservazione, conducono all'errore. Molta osservazione e poco ragionamento conducono alla verità"
(Alexis Carrel, Nobel 1912)

INDEX OF CONTENT

INDEX OF FIGURES

INDEX OF TABLES

INTRODUCTION

AIR POLLUTION

Air pollution exposure is a major problem worldwide and has been linked to many diseases. Air pollution consists of particulates, biological molecules or other harmful materials in the atmosphere that can cause health effects in human, and damage in living organisms and environment. The major sources of pollution are "*natural sources*", such as volcanic eruptions, forest fires, dust storms, bacteria and pollens or "*man-made sources"* such as vehicular traffic and industry. Pollutants are also classified in "*primary"* or "*secondary"*. Primary pollutants are emitted directly from a source into the atmosphere, the secondary ones are formed as a result of chemical reactions with other pollutants or atmospheric gases. For example, particle sulfates result from sulphur dioxide (SO_2) and ammonia (NH_3) gases reacting in the atmosphere. Commonly, emissions come from large stationary fuel combustion sources (i.e. electric utilities and industrial boilers), industrial and other processes (such as metal smelters, petroleum refineries, cement kilns, manufacturing facilities, and solvent utilization), and mobile sources including highway vehicles and non-road sources (i.e. recreational and construction equipment, marine vessels, aircraft, and locomotives). Sources emit different combinations of pollutants. For example, electric utilities release SO_2, NO_x, and particles fossil fuel combustion is the primary source contributing to CO_2 emissions. Major sources of fossil fuel combustion include electricity generation, transportation (including personal and heavy-duty vehicles), industrial processes, residential, and commercial [1]. Further classification can be made in relation to the physical state of pollutants. Gaseous contaminants include sulphur oxides (SO_x), nitrogen oxides (NO_x),

carbon monoxide (CO), volatile organic compounds (VOC) while solid pollutants include particulate matter (PM), persistent free radicals, toxic metals, chlorofluorocarbons (CFC_s) and ammonia (NH_3). The majority of these compounds can be grouped into five categories: sulfate, nitrate, elemental (black) carbon, organic carbon, and crustal material. In this work the attention was focused on particulate matter and its effects on the human health.

PARTICULATE MATTER COMPOSITION

Particulate matter (PM) characterizes a significant fraction of air pollution in the Earth's atmosphere and varies in size, shape, surface area, chemical composition, and can be of either natural or anthropological origin.

The size distribution of urban ambient particle pollution is usually characterized by the aerodynamic diameter (AED) which is defined as the diameter of a sphere of unit density (lg/cm^3) that has the same inertial properties in the gas as the particle of interest.

According to the size distribution, particulate matter is distinguished into: *coarse particles* (PM_{10}: 2.5 μm < d <10 μm), *fine particles* ($PM_{2.5}$: d ≤ 2.5 μm), or *ultrafine particles* ($PM_{0.1}$: d ≤ 0.1 μm) that includes also the nanoparticles (NP_S).

Primary particles and the precursor gases can have both *man-made* (anthropogenic) and *natural* (non-anthropogenic) sources. Mineral dust, metals, soot, salt particles, pollen, and spores constitute natural primary aerosols, while anthropogenic sources include combustion engines (both diesel and petrol), solid-fuel (coal, lignite, heavy oil and biomass) combustion for energy production in households and industry, other

industrial activities (building, mining, manufacture of cement, ceramic and bricks, and smelting), and erosion of the pavement by road traffic and abrasion of brakes and tires.

The process that formed secondary aerosols follow three steps that can increase particle size or modify its composition. Nucleation-mode is the first step in new particles generation [2] and depends on gases concentration, humidity, temperature in the atmosphere and transition of the gaseous phase to liquid or solid phase by condensation or chemical reaction, forming the first nuclei or particles in the atmosphere [3]. The second step is a condensation of hot gases, originating primary aerosols. This event is similar to nucleation. The final step in the aerosol formation is coagulation. Whole aerosols formed in previous steps can begin to agglomerate by Brownian motion [4] or turbulence and contact between particles. Consequently, particles grow in aerodynamic size forming secondary particles from primary particles (figure 1).

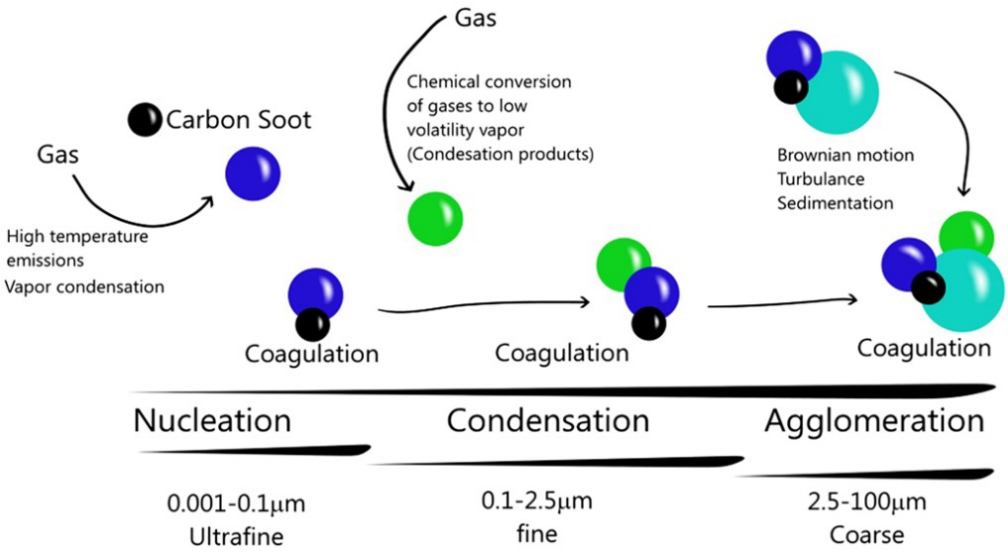

Figure 1. Particulate matter and its atmospheric dynamics. Particles nucleation is generated by gases emission. Condensation can occur by cooling, producing particles. The interaction between primary particles and secondary particles constitute the coagulation. In this way, the particles can increase their size and composition

The composition of PM is very complex and consists to metals, inorganic ions (SO_4^{2-}, NO^{3-}, Na^+, NH^{4+}, K^+) and volatile organic compounds coming from industrial chemicals such as fuels, solvents, coatings, feedstocks, and refrigerants (table 1). Furthermore, particle composition and concentration are extremely variable and depend on many factors such as climate variations, emission sources, and geographical position.

Metals are common components of PM and have been shown to interact with the immune system in antigen nonspecific fashion. Mishra et al. proposed that the generation of oxidative stress, either directly by transition metal components of PM or indirectly from the recruitment into the airspaces and activation of blood leukocytes, is a primary mechanism determining the inflammation-related health outcomes of PM [5].

The average daily values of $PM_{2.5}$ and PM_{10} concentrations might change from day to day mainly due to the thermodynamic conditions in the planetary boundary layer, which can either favour or adversely affect pollutants dispersion. Ambient weather conditions such as air temperature, relative humidity and short wave radiation can also influence chemical reactions leading to secondary aerosol formation.

In summertime, the higher average wind velocity and the broader mixing layer improve the dispersion of pollutants in the atmosphere while in winter, very frequent and persistent thermal inversions and fog situations at ground level cause a considerable amount of air pollutants to accumulate in the lower layers of the atmosphere [6].

Table 1. General particulate matter composition

COMPOSITION	ELEMENTS
Metals	K, Ca, Ga, Sr, Zr, Ba, Na, Li, Be, Ti, Sn, Mg, Al, Cs, Bi
Transitional metals	Cr, Mn, Fe, Ni, Cu, Zn, Cd, Au, V, Hg, Nb, Tl, Co, Mo, Zr, Rb, Ag
Non-metals	B, As, Se, S, Sb
Lanthanides and actinides	Sm, U, Tb, Ce, La
Biologicals	Glucans, Endotoxins, Pollens, Viruses
Carbon	Elemental and Organic
Policyclic Aromatic Hydrocarbons (PAHs)	(AcPy) acenaphtylene (Ant) anthracene (BaA) benzo[a]anthracene (BaFL) benzo[b]fluoranthene (BkFL) benzo[k]fluoranthene (BaP) benzo[a]pyrene (Bg,h,iP) benzo[ghi]perylene (BaP-TEQs) benzo[a] Pyrene-toxic (ChR) chrysene (Flu) fluorine (Fl) fluoranthene (Nap) naphthalene (InP) indeno[cd]pyrene (BkF) dibenzo[a,h]anthracene (Phe) phenanthrene
Others	Ammonium sulfates Ammonium nitrates Paraphormaldehyde

In a recent study, Marcazzan et al. examined the metals concentration in PM_{10} and $PM_{2.5}$ in Milan (figure 2) according to seasonal variation. In PM_{10}, S, Ca, Mn and Zn showed quite constant values; K, Fe, Br, Pb were lower in summer than in winter while Al, Si increased in summertime.

In $PM_{2.5}$, S, Mn, Cu, had similar values in winter and summer while K, Zn, Br and Pb Showed a decreased in summertime at the contrary to Al, Si, Ti, Ca, Fe that increased in the same season.

The percent increase of the typical soil-related elements Al and Si can be attributed to a greater soil dryness in summertime as well as to an increase in the mean wind speed, which fosters both the particles mechanical formation and their lift up. The decrease of some metallic elements in the summer period is essentially due to the lack of some sources (typically related to house heating) and to a better dispersion of the motor-vehicle emissions [7].

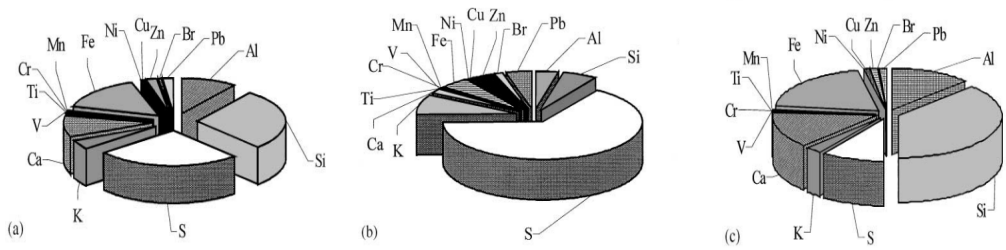

Figure 2. Relative contributions (in ng m^{-3}) of (a) PM_{10}, (b) $PM_{2.5}$, (c) PM_{tot}

PM AND HEALTH EFFECTS

Several studies have established a link between ambient air particulate matter (PM) exposure and health effects such as cardiopulmonary mortality and morbidity and lung cancer [8-15].

Some evidence suggests that ultrafine particles, soluble components from the particles, such as metals and organic substances, or inflammatory substances from the lung, may enter the circulatory system and act on the heart, the first encountered target organ beyond the lung. Airborne particulate matters, especially fine particles are able to absorb more toxic pollutants such as volatile organic compounds (VOCs), heavy metals,

polycyclic aromatic hydrocarbons (PAHs), biological components and carbonaceous materials [16, 17]. They were described as having the capacity to penetrate deeply into the human respiratory system [18, 19] and to reach the lung alveoli [20, 21] the air-blood gas exchanges head (figure 3).

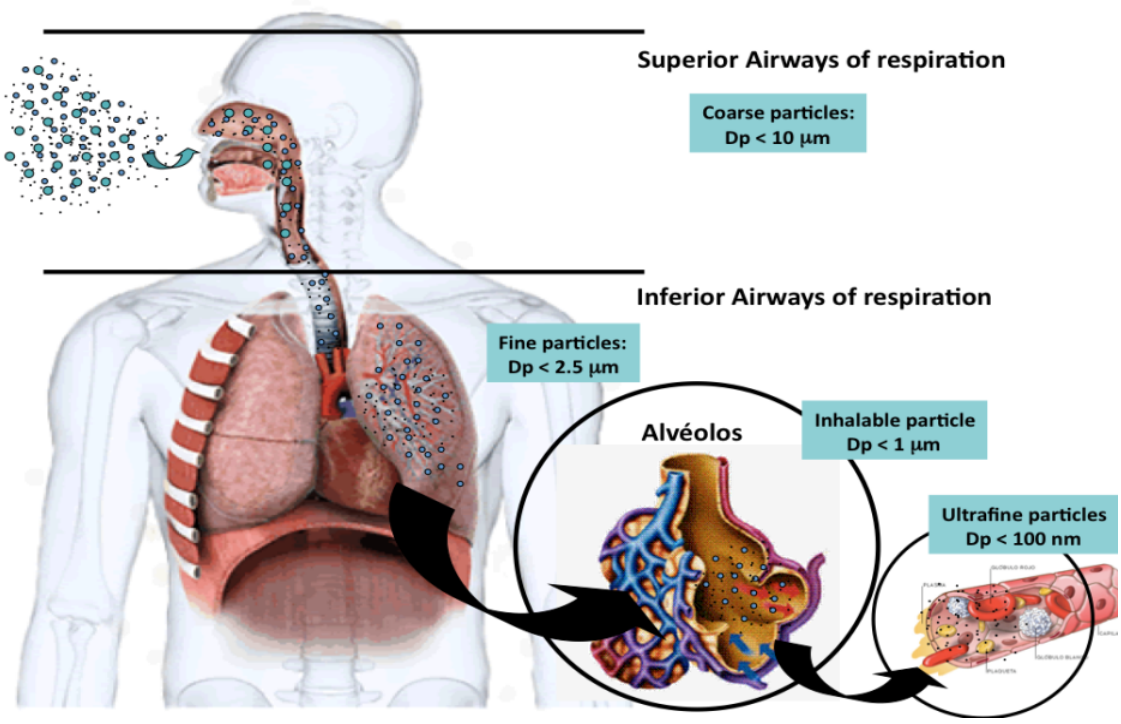

Figure 3. Size and dynamic particles in the lung and other tissues. Large particles can be deposited in upper airways through sedimentation or impaction while in the lower airways Brownian diffusion can deposit them in the alveoli. Ultrafine particles can translocate to blood-circulation and be deposited in the liver, spleen or brain. Although they might also penetrate through trans-synaptic mechanisms

Studies of air pollution exposure suggested that these particles have the ability to alter cell permeability by inducing production of reactive oxygen species and regulating the mediated responses (e.g. chemokine and cytokine secretion) in the lung airway [22-25]. In particular, a few epidemiological studies have shown an association between increased levels of inflammatory markers such as interleukin-6 (IL-6), C-reactive proteins (CRP), and coagulation factors, such as fibrinogen with coronary heart disease and mortality [26-28]. The inflammation seems to be a major determinant in PM-induced health effects. Alveolar macrophages and pulmonary epithelial cells constitute

the first line of defense against inhaled noxious compounds, and seem to play a central role in the out-break of inflammatory reactions upon PM exposure.

In the last decade, it has become increasingly clear that the health impact of PM is significantly affected by physical and chemical processes such as size, gas particle partitioning, hygroscopicity, redox kinetics, surface tension, molecular configuration, active sites, surface properties and chemical composition [29]. Several studies have shown that PM may be cytotoxic and may induce both apoptotic and necrotic cell death [30, 31]; this may be involved in the inflammation and development of both acute health effects and chronic lung diseases [32]. However, very little is known about the cellular, molecular and genetic/epigenetic alterations that may affect the incidence of chronic diseases in individuals exposed to PM.

PM AND OXIDATIVE STRESS

In a recent review Hussei et al. have highlighted emerging evidence of key biological and signal transduction pathways that trigger inflammatory and oxidative stress in response to PM exposure. Briefly, inflammation is induced by stress (chemical, physical), bacteria and viruses or environmental pollutants (e.g., cigarette smoke, air pollution) [33, 34]. The persistence of the inflammatory response can itself lead to tissue damage and thus drive many pathogenic processes including carcinogenesis and autoimmunity [35]. The ability of PM to induce an inflammatory response is dependent by the particle size [36]. Inhalational exposure to PM fine is commonly associated with enhanced pulmonary inflammation that is characterized by the rapid influx of neutrophils and induction of pro-inflammatory cytokines.

Oxidative stress and inflammation are closely related processes that can be induced by each other. Oxidative stress arises from an imbalance between oxidants and antioxidants that ultimately lead to the generation of reactive oxygen (ROS) and reactive nitrogen species (RNS) [37]. ROS are a class of molecules deprived of a complete electron pair and include free radicals and oxidants. Free radicals are generally small molecules with an unpaired electron in the outer valance and include the superoxide anion (O^{2-}), hydroxyl radical (•OH) and hydrogen peroxide. ROS are produced by all aerobic organisms during cellular respiration. In immune cells, such as neutrophils and mast cells, there is a respiratory burst and hence increased release of ROS.

Oxidative stress is one of the most common cellular outcomes associated with PM toxicity. Increased ROS due to exposure to PM have been shown in various cell types, including those of the respiratory system such as A549 [38, 39] and human lung fibroblasts [40, 41], those with relevance to cardiovascular disease include human aorta endothelial cells (HUVEC/HAEC) [42, 43] and macrophages [44].

Because they are highly reactive, ROS can damage key cellular components such as DNA, proteins, mitochondria and lipids. Thus, if cellular repair mechanisms cannot compensate for the excess oxidative stress and consequent cellular damage, then cell death can occur by necrosis (non-physiological) or apoptosis (programmed cell death) [45]. Indeed, exposure to PM increases oxidative stress and DNA damage with no compensatory upregulation of DNA repair in susceptible populations [46].

The production of ROS are counter-balanced with biochemical antioxidants [47]. A crucial part of the antioxidant system includes glutathione (GSH), a non-protein tripeptide assembled from cysteine, glutamic acid and glycine via the enzymes

glutamate cysteine ligase (GCL) and glutathione synthetase. Thiol groups present on the cysteinyl moiety of GSH react with oxidants and oxidized proteins, thereby detoxifying them. This reaction generates an oxidized dimer of GSH-GSSG that is reduced back to GSH by glutathione reductase. GSH participates in many important antioxidant defense pathways including the detoxification of superoxide (O^{2-}) via the enzyme superoxide dismutase (SOD). Indeed, there are significant perturbations in GSH levels with exposure to PM [48, 49]. Thus, an oxidant-antioxidant imbalance can lead to significant alterations within the cell that can culminate in enhanced cell death mechanisms.

The oxidative stress quantification is possible through indirectly markers of oxidation since the ROS species have high reactivity that makes their direct quantification very difficult. In the present work, 8-hydroxydeoxyguanosine (8-OHdG) and mitochondrial DNA copy number (mtDNA CN) were evaluated as major oxidative stress markers.

8-hydroxydeoxyguanosine (8OHdG)

Nuclear and mitochondrial DNA from tissue and blood lymphocyte is usually the site of oxidation damage [50]. Among all purine and pyridine bases, guanine is most prone to oxidation. Upon oxidation, a hydroxyl group is added to the 8^{th} position of the guanine molecule and the oxidative modified product 8OHdG (figure 4) is one of the predominant forms of free radical-induced lesions of DNA. Oxidative modified DNA in the form of 8OHdG can be quantified to indicate the extent of DNA damage.

In order to quantify 8OHdG in tissue or lymphocyte, enzymes such as endonuclease and glycosylase have to be used to cleave the oxidized product and release it into solution before they can be quantified. Increasing amounts of oxidative modified DNA have been detected in human tissues, particularly in tumors [51, 52].

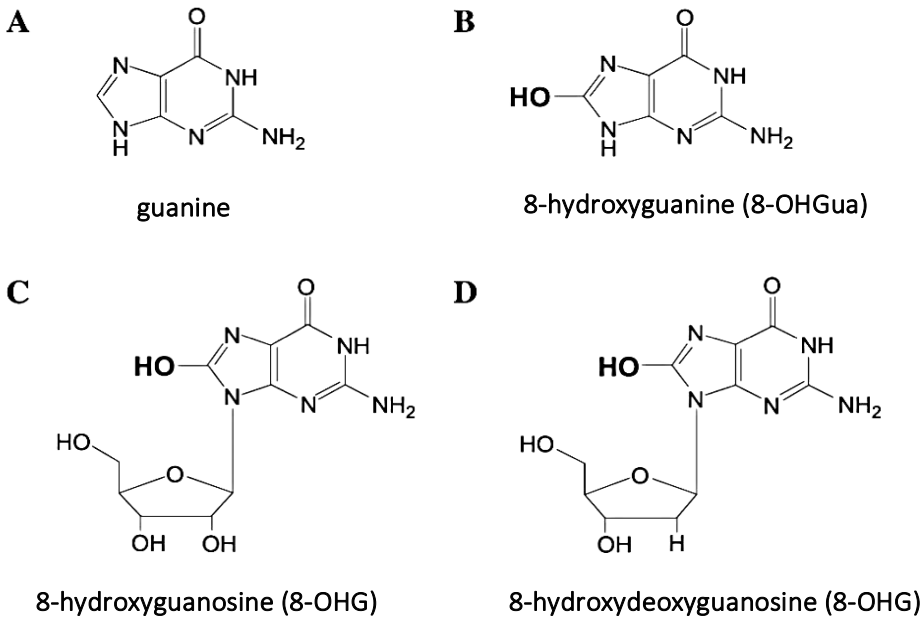

Figure 4. Chemical structure of 8OHdG and its analogues. (A) structure of an unmodified guanine base; (B) structure of an oxidized base; (C) analogue of 8OHdG derived from RNA; (D) structure of 8OHdG derived from DNA

Mitochondrial DNA copy number (mtDNA CN)

Human mitochondrial DNA (mtDNA) is a circular 16.569 bp, multicopy genome that encodes 13 polypeptides of the electron transport chain and ATP synthase (figure 5). Normal assembly and operation of the respiratory chain requires an intact and functional mitochondrial genome [53, 54]. The functional complement of mtDNA in a cell depends on both the copy number of mitochondrial genomes, which was first shown to be of the order of thousands per cultured mammalian cell [54], as well as the integrity of each mtDNA molecule. Many studies during the past decade have demonstrated somatic mtDNA mutations that accumulate with age [55, 56]. Human mtDNA is known to accumulate a variety of deletions that occur in all regions of the genome [57].

Various qualitative and quantitative assays have demonstrated an age-related increase in the incidence and abundance of mtDNA deletions of variable sizes and locations [62,64-65] which would be expected to reduce the complement of fully functional mtDNA.

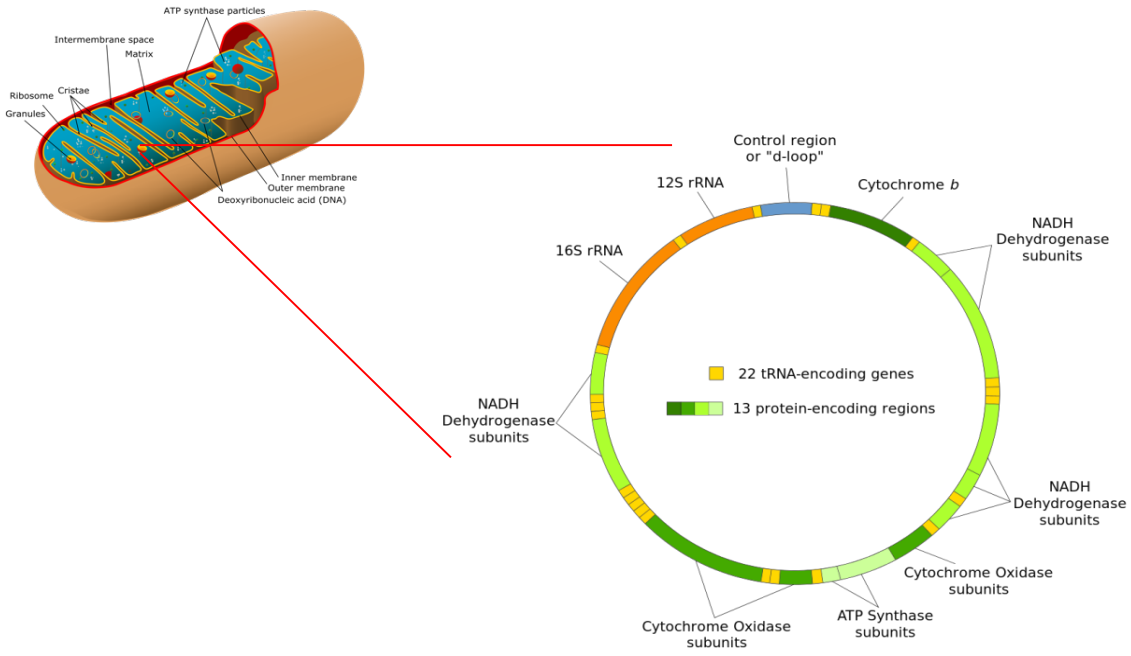

Figure 5. Mitochondrial DNA with groups of protein, rRNA and tRNA encoding genes

EPIGENETIC FACTORS

Genetics is the study of heritable changes in gene activity or function due to the direct alteration of the DNA sequence. Such alterations include point mutations, deletions, insertions, and translocation. In contrast, epigenetics is the study of heritable changes in gene activity or function that is not associated with any change of the DNA sequence itself. Although virtually all cells in an organism contain the same genetic information, not all genes are expressed simultaneously by all cell types. In a broader sense,

epigenetic mechanisms mediate the diversified gene expression profiles in a variety of cells and tissues in multicellular organisms [58].

These changes may induce phenotypic changes and persist through cell divisions for the remainder of the cell's life, possibly lasting for multiple generations without any change in the intrinsic DNA sequence of the organism. The most investigated epigenetic marker is DNA methylation.

DNA methylation

DNA methylation is an epigenetic mechanism involving the transfer of a methyl group onto the C5 position of the cytosine to form 5-methylcytosine (5MeC), heritable by somatic cells after cell division (figure 6). DNA methylation regulates gene expression by recruiting proteins involved in gene repression or by inhibiting the binding of transcription factor(s) to DNA [58].

5- methyl-cytosine (5MeC) represents 2-5% of all cytosines in mammalian genomes and is found primarily on CpG dinucleotides, often located in enriched regions called CpG islands. Around 60% of the promoters of protein-coding genes in the human genome seem to contain CpG islands, and most of them appear methylated in differentiated tissues [59]. DNA methylation is controlled by DNA methyltransferases (DNMTs), which catalyse the transfer of a methyl group from the methyl donor, S-adenosyl methionine, into the 5′ position of the cytosine ring. They consist of a C terminal catalytic domain and an N terminal regulatory domain.

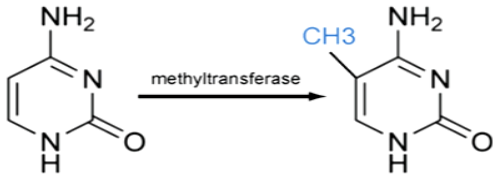

Figure 6. The chemical mechanism in DNA methylation

5 mammalian DNMT's have been identified, however, only DNMT1, DNMT3A and DNMT3B have conclusively been shown to exhibit catalytic activity [60]. DNMT1 is the "maintenance" methyl-transferase and its role is to maintain the correct methylation pattern during DNA replication occurring in the cellular cycle. DNMT3a and DNMT3b are responsible for the de novo establishment of DNA methylation patterns after implantation [61] (figure 7). The extent of DNA methylation changes in an orchestrated way during mammalian development, starting with a wave of demethylation during cleavage, followed by genome-wide de novo methylation after implantation.

The methylation status of a gene is usually inversely correlated with gene expression, so that hypermethylation of certain gene promotors yields gene inactivation, and hypomethylation of these promoters activates or reactivates gene expression [62, 63]. DNA methylation seem to be involved in both initiating gene silencing as well as maintaining it. An increased methylation, in fact, leads to transcriptional repression as it inhibits the binding of transcription factors to their cognate DNA recognition sequences or because it recruits methyl–CpG-binding proteins (MeCPs and MBDs) together with co-repressor molecules [63]. CpG islands in promoters of housekeeping genes are physiologically hypomethylated and therefore transcriptionally active. The re-

expression of hypermethylation silenced genes in the presence of the demethylating agent, 5-azacytidine, has been demonstrated for many genes [64, 65].

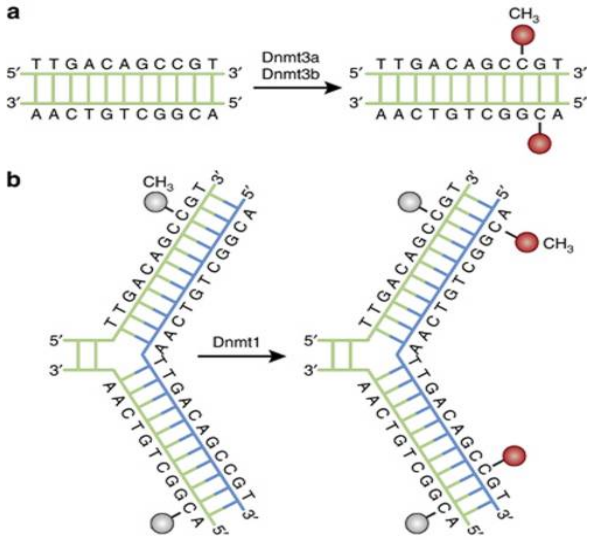

Figure 7. DNA methylation pathways. DNA methyltransferases (Dnmts) catalyses the transfer of a methyl group from *S*-adenyl methionine (SAM) to the fifth carbon of cytosine residue to form 5-methylcytosine. (a) Dnmt3a and Dnmt3b are the *de novo* Dnmts and transfer methyl groups (red) onto naked DNA. (b) Dnmt1 is the maintenance Dnmt and maintains DNA methylation pattern during replication. When DNA undergoes semiconservative replication, the parental DNA stand retains the original DNA methylation pattern (gray). Dnmt1 associates at the replication foci and precisely replicates the original DNA methylation pattern by adding methyl groups (red) onto the newly formed daughter strand (blue)

Telomere length (TL)

Telomere length (TL) has been evaluated since increased oxidative stress has been associated with telomere integrity [66]. Telomeres were defined in the 1930s as essential components that stabilize chromosome ends (figure 8). Telomeric dysfunction due to excessive shortening is a key element leading to chromosomal instability [67]. Telomeres are DNA repeat sequences (*TTAGGG*) that, together with associated proteins, form a sheltering complex that caps chromosomal ends and protects their integrity [68]. Due to the limitation of DNA polymerase (telomerase), genetic stability is gradually lost as telomeres are shortened with each round of cell division [68, 69].

In addition, telomeric erosion can be further accelerated by external stressors. Telomeres, as triple-guanine-containing sequences, are highly sensitive to oxidative stress [70], alkylation [71] or ultraviolet irradiation [72]. The resulting damaged telomeric bases by double-strand breaks and/or interference with replication fork may induce a reduction in telomere length (TL)[73].

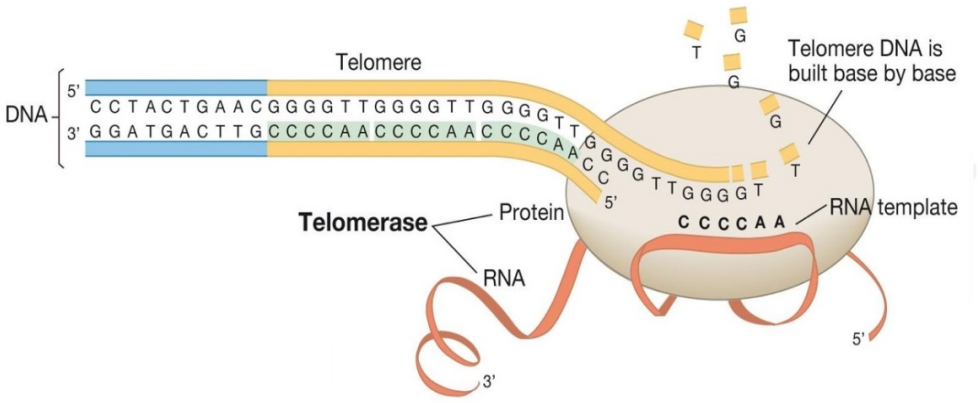

Figure 8. Telomere structure

VIRUS DNA METHYLATION

Epstein-Barr virus (EBV)

Epstein-Barr virus (EBV) is a herpesvirus, present in about 90% of the world's population [74]. Primary EBV infection is generally acquired during adolescence causing infectious mononucleosis (IM). After the infection of oropharynx epithelium and naïve B cell [75], EBV persists latently in infected B cells for the lifetime of the infected individual, residing as a multicopy episome and replicating with each cell division [76].

Indeed, the primary infection activates the B cell, leading to proliferation through its latency III program, in which it expresses all latency genes: latent membrane proteins (LMP1 and LMP2), EBV nuclear proteins (EBNA1, 2, 3A, 3B, 3C and LP), Epstein-Barr encoded RNAs (EBER1 & EBER2) and BAMHI A rightward transcripts (BARTs).

Once infected, the B-cells migrate to the follicle where the latency program switches to latency I/II in the germinal centre. Latency-I occurs during memory B cell division and only EBNA1 is expressed. In latency II LMP1, LMP2, EBERs and EBNA1 are expressed. EBV is maintained within memory B cells in the form of an episome where the latency program switches to latency 0 during which no viral proteins are expressed. The Epstein-Barr virus latent cycle promoter Wp drives expression of EBNAs at the initiation of virus-induced B-cell transformation in vitro. Thereafter, Cp promoter becomes dominant in the EBNA expression when Wp activity decreases dramatically [77]. In latency-I, Cp and Wp are inactive and EBNA1 is expressed from Qp.

For reactivation and virus replication, the infected B cell can differentiate into a plasma cell, which induces replication and these cells can home to the tonsillar epithelium, allowing the transmission of EBV through the saliva secretion.

Generally malignant tumours such as Burkitt Lymphoma and Nasopharyngeal carcinoma have latent EBV infection but there can be a small amount of EBV lytic cycle reactivation and this is also seen in multiple sclerosis patients. Two immediate-early (IE) genes, BZLF1 and BRLF1 are responsible for the switch from latent to lytic infection. Histone acetylation in the Zp (*BZLF1*) and Rp (*BRLF1*) promoters is a key mechanism of physiological reactivation but hypermethylation of promoters in EBV-positive cell lines can play a role in silencing lytic cycle gene expression, which may be reactivated by some demethylation agents and ultimately initiate the EBV lytic cycle [78] (figure 9).

Epigenetic mechanisms as DNA methylation are important regulators of the EBV cycle, determining different type of infections [79, 80]. DNA methylation can be sensitive to environmental factors such particulate matter (PM_{10}) and previous studies showed a

correlation between the exposure to particulate matter and change in DNA methylation of EBV [78, 81-83].

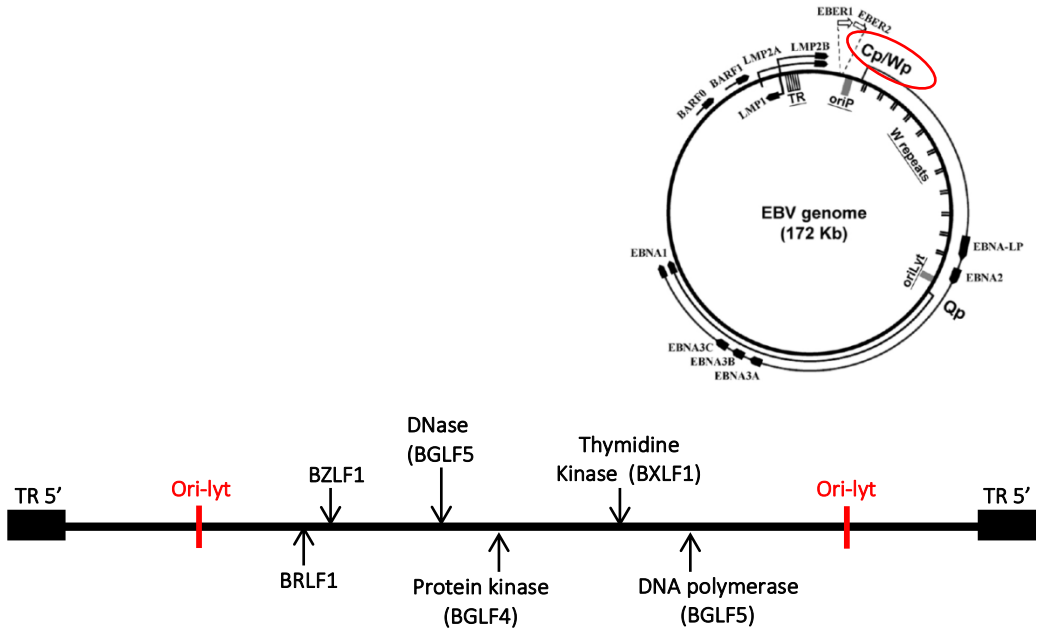

Figure 9. EBV genome in episome form including Wp/Cp sequences (*above*) and BZLF1 protein (*under*) sequence analysed in the study

Human endogenous retroviruses (HERV-w)

Sequencing of the human genome has revealed that approximately 2% of the genome is composed of protein-coding regions, whereas approximately 8% of our DNA is recognized as containing human endogenous retrovirus (HERV) elements [84, 85] and they are well-known regulators of the immune system [86]. Based on sequence similarities HERVs can be grouped into at least 31 families, one of which is the w family of HERV [87]. As other HERVs, a HERV-w provirus has a prototypical retroviral structure, that is, internal *gag, pol* and *env* genes flanked by two intact 780-bp long terminal repeats (LTRs). LTRs contain a range of regulatory sequences such as effective promoters, enhancers, and transcription factor-binding sites [88].

The LTR is composed of U3, R, and U5 regions. The U3 region of the 50 LTR acts as proviral promoter, while the R region located in the 30 LTR serves as a polyadenylation

signal. Apart from proviral elements, HERV-w contains pseudoelements, bearing the hallmarks of processed pseudogenes, and elements that only display partial internal sequences due to extensive deletions/truncations (figure 10).

Pseudoelements, probably representing LINE-1-mediated retrotransposition of proviral transcripts, lack the U3 region of 50 LTR, and the U5 region of 30 LTR. The HERV-w pseudoelements are typically characterized by their co-linear structure with retroviral mRNA followed by poly(A) tails. In contrast to very few detected pseudoelements in other HERV families (for instance < 1% of HERV-h are pseudoelements), a large proportion of pseudoelements (25%) have been observed in HERV-w which distinguishes it from other HERV families [88, 89]. DNA methylation is directly involved in the transcriptional regulation of HERV elements, which is extensively altered in many type of cancers and diseases [90, 91]. Infectious agents can also trigger transactivation of members of the HERV-w family. Activation of HERV-w by herpes virus simplex type I (HSV-1) infection mediated by its immediate early protein 1 (IE1) has been observed indifferent diseases as schizophrenia [92], and sclerosis [93]. Moreover, recent studies revealed a relation between EBV and HERV-w expression, as EBV reactivation might be able to induce HERVs expression [94, 95].

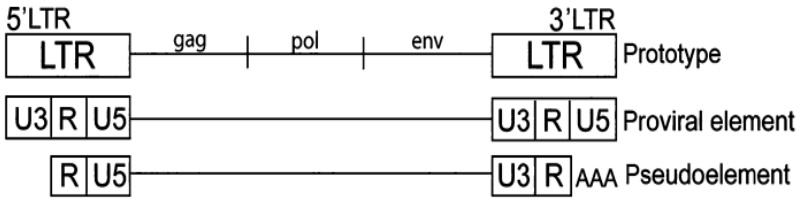

Figure 10. Schematic illustration of the HERV-w structures

EXTRACELLULAR VESICLES

Intercellular communication is an essential hallmark of multicellular organisms and can be mediated through direct cell–cell contact or transfer of secreted molecules. In the last two decades, a third mechanism for intercellular communication has emerged that involves intercellular transfer of extracellular vesicles (EVs). The release of apoptotic bodies during apoptosis has been long known [96], but only recently the fact that also healthy cells shed vesicles from their plasma membrane become acknowledged.

Circulating vesicles (EVs) are composed of exosomes and microvesicles (MVs)(figure 11). Microvesicles are extracellular vesicles (size from 100-1000 nm) with different shapes. They are formed by regulated release of outward budding of the plasma membrane, consequently they also express antigenic markers of the cell from which they originate.

The generation of MVs is dependent on both the cell and the stimulus, with lipid bilayer rearrangement (or derangement) that represents a critical component of MV formation [103].

Exosomes (diameter range from 40 to 100 nm) are homogeneous shape that originate from inward budding of the limiting membrane of multivesicular bodies, which are late endosomal compartments present in the cytosol of the cell. When the multivesicular bodies fuse with the plasma membrane they release exosomes to the extracellular space, causing the orientation of the membrane proteins to be similar to that of the plasma membrane. They are now known to be involved in numerous endocytic and trafficking functions, including protein sorting, recycling, transport, storage, and release and their production is stimulated in response to alterations in the microenvironment [97, 98].

There are some resemblances between microvesicles and exosomes: both carry proteins, mRNA, and microRNA (miRNA) and are involved in cellular communication [101, 102], possibly through the horizontal transfer of genetic material, directly stimulating the target cell by transferring receptors or proteins [99, 100].

Even more attention was given to extracellular vesicles (EVs) as a very credible link, in to intercellular and between-tissue communication [101] as they can travel from the tissue of origin to target cells, transferring their contents after being internalized [102].

Recent studies support the possible role of EVs as a very promising molecular mechanism pivotal in stimulating the systemic response to PM exposures [103] showing that elevated numbers of EVs in healthy subjects were linked to increased risk for developing CVD [104, 105] and that EVs are probably powerful intercellular messengers in CVD, reviewed in [106].

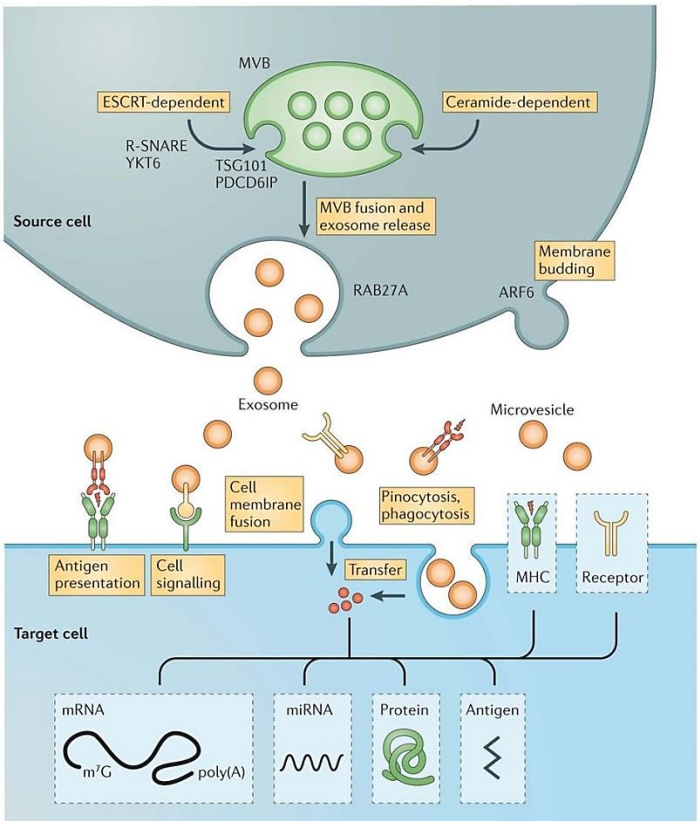

Figure 11. Biogenesis of extracellular vesicles and their interactions with recipient cells

STUDY RATIONALE AND AIMS

Exposure to particulate matter is associated with increased incidence of several diseases, but the molecular mechanisms underlying these associations remain unknown. Obesity may increase susceptibility to the adverse effects of PM exposure, exacerbating the effects of PM on human health. Extracellular vesicles (EVs), which travel in body fluids and transfer molecular messages among tissues, might play an important role in connecting external exposures to health effects.

In a previous study conducted by Bonzini et al [107], on the same study population we are currently investigating, we observed a positive association between short term PM_{10} and $PM_{2.5}$ exposure and EVs concentration in plasma. PM-induced EVs alterations in overweight subjects (BMI >25) were more pronounced, with visible effect in all EV subtypes, particularly EVs derived from endothelial cells.

Starting from this preliminary observation, we hypothesized a cascade of events connecting PM exposure to molecular alterations (viral sequence methylation and telomere length modification), through a modulation of oxidative stress markers (mtDNA CN and 8OHdG). This cascade could potentially be triggered by EV release induced by PM exposure. Our original hypothesis was to investigate EVs as carriers of information from pulmonary environment to peripheral cells but also as carriers of smaller components of exposure (i.e. metals).

Unfortunately, the method we developed and validated to assess EVs metal content was not applicable to our study population, as it requires more plasma than available (1.5 ml). For this reason, the majority of metals examined were below the limit of detection and prevent any further analyses.

The specific aims of the present study (figure 12) were:

1. set up and validate an analytical method to measure metals in EVs;
2. to investigate in healthy subjects whether air pollution exposure can modify:

a) Oxidative stress markers such as 8-hydroxy-2'–deoxyguanosine (8OHdG) and mitochondrial DNA copy number (mtDNA CN) which might be an intermediate mechanism linking altered EVs trafficking to epigenetic alterations.

b) Telomere length modification in peripheral blood mononuclear cells (PBMCs), possibly related to oxidative stress levels.

c) Alterations in HERV-w and EBV methylation in PBMCs, as global hypomethylation, frequently related to PM exposure, has been associated to viral sequence reactivation, possibly linked to the activation of pro-inflammatory pathways occurring after exposure.

3. To further confirm in vitro the effect of PM on EBV regulation.

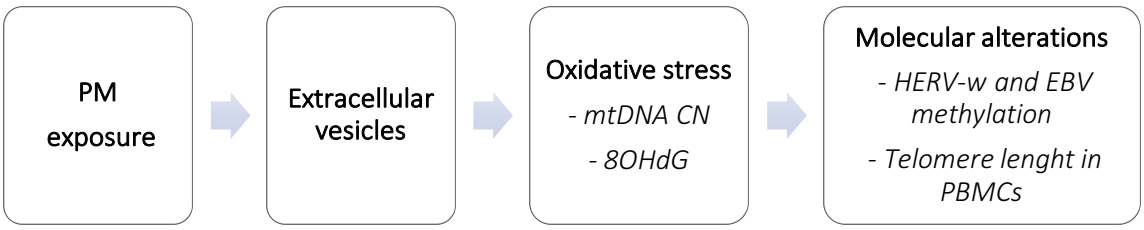

Figure 12. Possible cascade of events linking PM_{10} exposure to molecular marker alterations

The three aims detailed above, have been deepen in the three main sections of this thesis.

SECTION I: Validation of an analytical method for metal quantification in extracellular vesicles;

SECTION II: Epidemiological study to evaluate epigenetic and molecular outcomes after PM exposure;

SECTION III: Epstein-barr virus reactivation after PM exposure - in vitro studies.

SECTION I: VALIDATION OF AN ANALYTICAL METHOD FOR METAL QUANTIFICATION IN EXTRACELLULAR VESICLES

In the first part of PhD project, we developed a method for the metals quantification in extracellular vesicles (EVs) of a pool of healthy blood donors. The EVs were extracted of a plasma healthy subjects recruited at the IRCCS Ca' Granda Ospedale Maggiore, Policlinico.

In according to IUPAC 17025 guidelines, analytical parameters as *accuracy, precision, sensitivity, limit of detection, (LOD) limit of quantification (LOQ) and, matrix effect* were evaluated in validation method for 7 metals: Chromium (Cr), Nickel (Ni), Manganese (Mn), Cobalt (Co), Iron (Fe), Copper (Cu) and Zinc (Zn) in EVs.

The most critical part of this work has been to identify and eliminate possible heavy metals sources, which may be the cause of error in quantification of metals in extracellular vesicles. We considered the contribution of metals supplied by the laboratory materials and solutions used to extract the EVs. In particular, we identified some critical steps as:

- falcon and vials used during centrifuge and ICP-MS analysis respectively,
- solution phosphate buffered saline (PBS) used for suspending EVs after centrifuge,
- tube topper used for close vials before ultracentrifuge.

These evaluations have led to the replacement of phosphate solution buffer PBS, with the physiological solution, and the washing with HNO_3 for ultracentrifuge vials, for reduce Fe, Cu, Zn supplement.

LOD and LOQ determination was done for each sample using calibration curve in nitrile acid at 0.65% showing the minimum value determinable for each metal.

The matrix effect was evaluated to determine the influence of matrix components (EVs) on analyte quantification (metals). Briefly, a curve with 100 µl microvesicles was prepared and compared with a standard calibration curve. The slope difference showed a ratio to 1 indicating a minimum matrix effect.

MATERIAL AND METHODS

Extracellular vesicles extraction

Peripheral blood, collected in two EDTA tubes (processed within 4-hr) were centrifuged at 1.200 x g for 15 minutes at room temperature. After centrifugation, the intermediate stage (buffy coat), consisting mainly of lymphocytes and monocytes, was isolated and frozen. To prepare EVs pellets for metals quantifications, 1.5 mL of fresh plasma was transferred to an ultracentrifuge tube (Quick-Seal, Round-Top, polypropylene, 13.5 mL; Beckman Coulter, Inc., Indianapolis, IN, USA), which was then filled up with physiological solution to minimize metals contribution on the background particles.

Plasma was then spun in a benchtop ultracentrifuge (Optima MAX-XP; Beckman Coulter, Inc.) at 110,000× g for 75 min at 4°C, to obtain an EVs pellet and frozen at -80° C until further analysis.

Sample preparation for metals quantification

Before the analysis, EVs pellet were treated with HNO_3 to remove the organic matrix and reduce non-spectral interferences or matrix effects. Briefly, 100 µl of EVs was treated with 25 µl of an aqueous solution of nitric acid 40% V/V prepared by dilution of 5.7 ml to ultrapure acid (69% traceselect, Fluka, France) into 10 ml to Milli-Q® ultrapure water (conductivity 0.056 µs/cm) (Merck, Darmstadt, Germany).

After 1 hour with acid digestion EVs samples were added with 1 ml of a solution prepared by 360 µl of a solution containing 0.6 µg/ml of ^{45}Sc, ^{89}Y, ^{111}In as internal standards (Inorganic Ventures, Inc., Lakewood, NJ, USA). All samples were mixed and centrifuged for 30 min at 16.000 rpm.

The supernatant was eluted into 2.4 ml of an aqueous solution and analysed by inductively coupled plasma-mass spectrometry X Series II (Thermo Electron Corporation, Rodano, Italy).

Metals quantification by inductively coupled plasma-mass spectrometry (ICP-MS)

Inductively coupled plasma (ICP) mass spectrometry (MS) is one of the most powerful techniques for trace and ultra-trace analysis of elements in different fields (medicine, biology, chemistry, environmental etc.).

The samples to be analyzed is introduced into the hot core of the plasma through the central tube by means of a stream of argon carrier gas. The samples are in aerosol form generated by nebulization of the sample solution. At the end of plasma burner, a high frequency signal from a coil is coupled with the argon flow and the inductively coupled plasma is thus generated. The temperature up 8000 K, which occur in plasma permit the decomposition of molecules into ions. Therefore, a small portion of polyatomic and multiply charged ions are also generated. These ions are transferred via a plasma interface, which consists of orifices (*cones*) and a differential pumping system with several pressure stages, from the plasma which is it an atmospheric pressure into a vacuum of 10^{-8} to 10^{-10} bar. The ions are separated in quadrupole and are then quantified by means of a detector (figure 13).

In mass spectrometry, mass/charge ratio (*m/e*) are analysed. Normally e=1 (single charged ions), but depending on the ionized energy, ions bearing double or even multiple charges can occur. All the other ions are discharged at one of the four roads of the quadrupole [108]. In order to optimize the performance of the instrument, and

optimum conditions are chosen for the nebulizer (transported sample amounts and aerosol carrier gas) and ICP (power of the introduction coil and a various gas flows).

The inductively coupled plasma-mass spectrometry (ICP-MS) X Series II (Thermo Electron Corporation, Rodano, Italy) equipped with standard nickel cones, torch, and quartz impact bean spray chamber and interfaced to an auto sampler ASX-100 (Teledyne CETAC Technologies, Omaha, NE, US) was used in this study.

The instrument was operated with standard mode for copper and with reaction mode (CCT-Ked) for chromium, manganese, iron, cobalt, nickel and zinc.

The standard mode conditions were as follow: extraction voltage was -100 V, focus voltage 10 V, nebulizer gas flow rate 0.90 L/min, dwell times was 10 ms for each element. For each sample, three replicates were run. In collision cell mode (CCT-ked), a cell gas flow of 3.5 ml/min of 8% V/V Hydrogen in Helium was used to reduce interferences.

Before each analytical sequence, the instrument was calibrated using the tune solution obtained by dilution 1:50 of the multi-element solution Tune A (containing Ba, Be, Ce, Co, In, Li, Ni, Pb, each at 10 mg/ml in 5% HNO3) (Analytika, Prague, Czech Republic). The calibration curves were in the range 0.02- 2.5 µg/L for Co, Cr, Mn, Ni, and 2.5-100 µg/L for Fe, Cu and Zn. The calibration solutions were obtained by dilution of the multi-element standard stock solution 71A, containing all elements analysed at 10 mg/ml (Inorganic Ventures, Inc., Lakewood, NJ, USA), using an aqueous solution of nitric acid 0.05% V/V containing 45Sc, 89Y, 111In, at 6 µg/L as internal standards. The calibration curves for each metal were linear with correlation coefficient ≥0.999. The limits of quantification (LOQs), calculated as ten times the standard deviation of the blank, were in the range 0.26 - 4.5 µg/L.

Internal quality assurance was performed using two quality controls (QCs) for metals in plasma: Seronorm® Level-1 and Level-2 (Sero AS, Billingstad, Norway). Before analysis, these controls were reconstituted according with manufacture's instruction. The accuracy for quality controls was between 86 and 113% and the precision was between 2 and 9%.

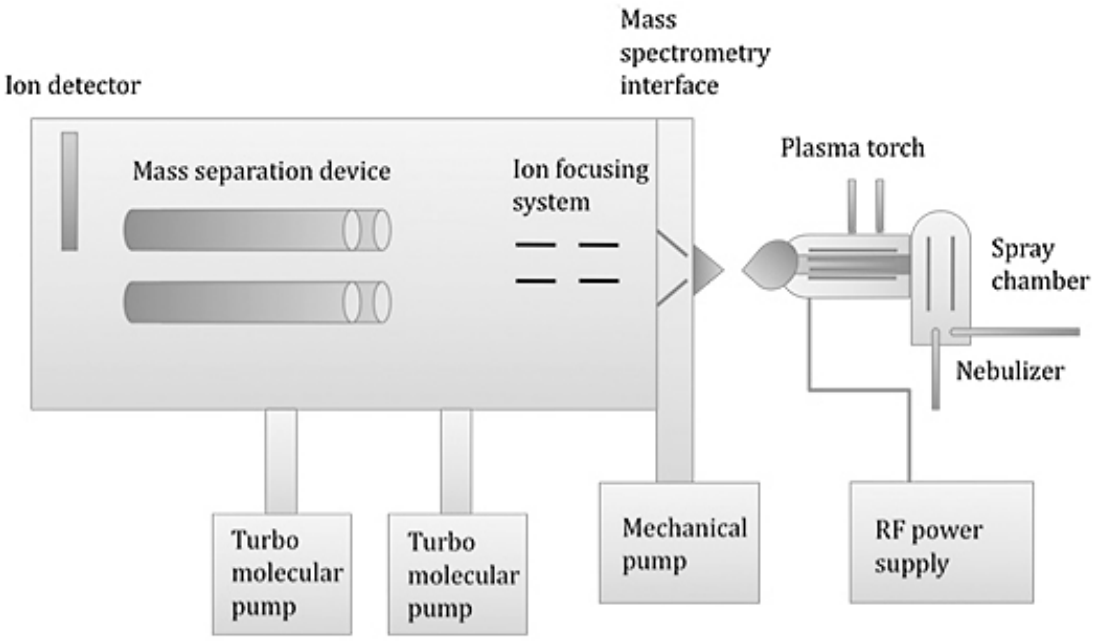

Figure 13. Schematic ICP-MS diagram

RESULTS

The validation method was obtained setting the optimal instrumental condition for high sensibility and stability during EVs analysis. Limit of detection (LOD) and limit of quantification (LOQ) were evaluated for each metal. The coefficient of correlation was more of 0.999 for all metals studied and recovery amount 70%. The reproducibility or cv% was between 5 and 10%. The analysis was elaborated with Plasma Lab software (Thermo-Fisher Scientific, UK).

The method has been validated using EVs extracted from blood donor's volunteers achieving the first purpose of this part of the study.

However, EVs extracted from 50 blood samples collected by healthy subjects recruited at the IRCCS Ca' Granda Ospedale Maggiore, Policlinico showed a metal content too low compared to instrumental LOD and LOQ (table 2).

A future step to resolve this limit could be to collect a higher volume of 100 µl EVs for increase the ICP-MS atomization and consequently a higher metals concentration detection.

Table 2. Limit of detection (LOD) and limit of quantification (LOQ) for metals in relation with metals concentrations in EVs.

METALS	LOD *(µg/L)*	LOQ *(µg/L)*	EVs* *(µg/L)*
Chromium	0.04	0.09	0.02
Manganese	0.10	0.15	0.14
Iron	0.84	1.69	6.2
Cobalt	0.1	0.2	0.006
Nickel	0.05	0.10	0.09
Zinc	0.7	1.4	0.6

* metal concentrations in MVs were lower than LOD and/or LOQ.
The EVs metals concentrations were reported as examples to 50 samples analyzed.

SECTION II - EPIDEMIOLOGICAL STUDY TO EVALUATE EPIGENETICS OUTCOMES AFTER PM EXPOSURE

MATERIAL AND METHODS

Study subjects

The study population included 50 healthy volunteers recruited at the IRCCS Ca' Granda Ospedale Maggiore, Policlinico from November 2014 to March 2015. This period of the year is characterized by high levels of air pollution in Northern Italy due to mainly traffic exhaust emissions and residential heating combined with peculiar meteorological changes [109].

After signing a detailed informed consent form, each volunteer has worn miniaturized personal sampling device to measure PM_{10} and $PM_{2.5}$ for 24-hr, beginning at 9 AM (day -1). After one day, to each subject venous blood drawing at 9 AM (day -2) was done. During the monitored 24-hr, subjects were invited to perform their routine activities.

All participants also completed a questionnaire collecting detailed personal data, including anthropometric characteristics (e.g., height and weight, BMI), education, area of residence, job position and location, time spent commuting in traffic, alcohol consumption, smoking habits, drugs, and pre-existing medical conditions.

Exposure assessment

Personal Exposure

The subjects' personal exposure to PM_{10} and $PM_{2.5}$ was measured with a miniaturized personal cascade impactor sampler (PCIS; SKC Inc., Eighty Four, PA, USA). The sampler

consisted of four impaction stages with cut-off diameters of 2.5, 1.0, 0.5, and 0.25 μm followed by a backup filter stage for particles <0.25 μm.

Stretch polytetrafluoroethylene/polytetrafluoroethylene (S-PTFE/PTFE) filters (25 mm diameter and 0.8 μm porosity) were used as impaction substrates, and the backup filters were PTFE w/polymethylpentene ring membranes (37 mm diameter and 2 μm porosity). For this study, the original sampler was modified by excluding the 1.0, 0.5, and 0.25 impaction stages. A field inter-comparison test was performed to verify the agreement between the original and the modified configuration. The resulting mean relative error was < 1%.

PM concentrations were determined by gravimetric analysis. The net PM mass was obtained by weighing filters before and after sampling with a microbalance (Micro 1000; Gibertini, Novate, MI, Italy) inside a temperature- and relative humidity-controlled (20 ± 1°C, 50 ± 5%) cabinet (Activa Climatic; Aquaria, Lacchiarella, MI, Italy). Quality of the weighing procedure was assessed using the American Society of Testing and Materials D 6552 method. The limit of detection was 9 μg and 5 μg for PM_{10} and $PM_{2.5}$, respectively, which approximately corresponds to 0.7 $\mu g/m^3$ and 0.4 $\mu g/m^3$, respectively, for 24-hr samplings at 9 L/min. The PM sampler was connected to a sampling pump (Leland Legacy; SKC Inc.) operated at a flow rate of 9 L/min and carried by subjects in the breathing zone. During night time, the instruments were placed in the living room.

Under the hypothesis that variation in epigenetic markers due to environmental stimuli are commonly observed in short time lags, we chose to investigate a 1-week lag exposure time window before Day 0. As PM exposures obtained by PCIS [103], was limited to the 24-h average exposure before blood collection (Day-1 PM), we integrated

the PM_{10} and $PM_{2.5}$ daily average exposures using data obtained from Air Quality Monitoring Network of the Regional Environmental Protection Agency (ARPA Lombardia) (Day-1 PM to Day-7 PM).

We collected PM daily levels from the available fixed ARPA monitoring stations (MS). Using ArcGIS® software by Esri, we assigned to each subject the daily PM concentration from the nearest monitor to home address for the 7 days preceding blood sampling. We also obtained ARPA Chemical Transport Model (CTM) that provides daily PM concentration estimates with municipality resolution. During the study period (2014-2015), CTM was available only for PM_{10} estimation, accordingly $PM_{2.5}$ estimations were collected using PM daily levels from the available fixed ARPA monitoring stations (MS).

Sample processing

DNA extraction and quality control

Seven millilitres of whole blood were collected into EDTA tubes from each participant and promptly centrifuged on site at 2.500 rpm for 15 min. The buffy coat (≈200 µL) was transferred in a cryovial, immediately frozen in vapour phase of liquid nitrogen, and shipped in nitrogen dry shippers to the laboratory. DNA was extracted using the Wizard Genomic DNA purification kit (Promega, Madison, WI, USA) following the manufacturer's instructions. Extracted DNA was resuspended in sterile deionised water DNA concentration was calculated using Nanodrop at a wavelength of 260 nm.

Real time polymerase chain reaction RT-PCR

The Real-Time Polymerase Chain Reaction (RT-PCR), monitors the amplification of a targeted DNA molecule during the cycles of PCR, i.e. in real-time, and not at its end, as in conventional PCR. In RT-PCR the amount of DNA is measured after each cycle by the use of fluorescent markers incorporated into the PCR product; the increase in fluorescent signal is directly proportional to the number of PCR product molecules (amplicons) generated in the exponential phase of the reaction. Fluorescent reporters include: i) non-specific fluorescent dyes that intercalate with any double-stranded DNA (Syber Green, Eva Green) and ii) sequence-specific DNA probes consisting of oligonucleotides that are labelled with a fluorescent dye, which permits detection only after hybridization of the probe with its complementary sequence.

In this study, we used Syber Green fluorescent dye (figure 14), and we add to each run a Melting Curve Analysis to evaluate the specify of the reaction. A Melting Curve charts the change in fluorescence observed when double stranded DNA (dsDNA) with incorporated dye molecules dissociates, or "melts", into single strand DNA (ssDNA) as the temperature of the reaction is raised.

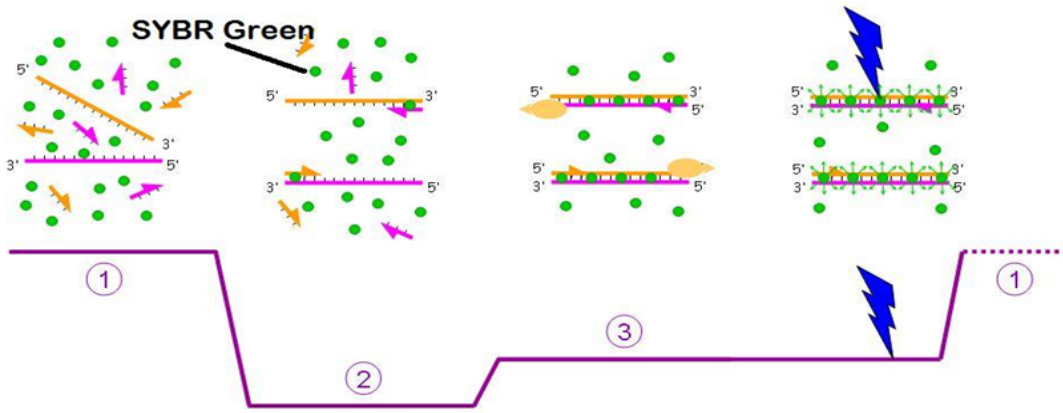

Figure 14. SYBR Green in qPCR cycle. At the beginning the double strand is denaturant in two single strand (1). During primer annealing (2) SYBR GREEN upon binding to double-strand DNA emits fluorescence very brightly. In the extension phase (3) SYBR signal intensities correlate with DNA amplified (amplicon amount) and thus the initial sample input amounts.

8OHdG quantification

Mitochondrial 8-hydroxy-2-deoxyguanine (8OHdG) was measured using RT-PCR as previously described. Treatment with the human 8-oxoguanine DNA N-glycosylase 1 (hOGG1) enzyme is responsible for the excision of 8OHdG. Briefly, 4 µl of DNA sample (25 ng) was treated with 11 µl treatment mix containing RNase free water (8.7 µl/reaction), buffer NE 10× (1.5 µl/reaction), BSA 100× (0.15 µl/reaction), and the enzyme hOGG1 or RNase free water (0.625 µl/reaction) for the treatment mix and non-treatment mix respectively.

After an incubation of 1 h at 37 °C, samples were diluted 1: 4 in RNase free water and a fragment of mtDNA (*MT-ND1*- subunit of NADH dehydrogenase) was amplified by qPCR using a master mix consisting of Fast SYBR® Green I dye 2× (5 µl/reaction), forward (0.5 µl/reaction) and reverse (0.5 µl/reaction) primers (MT-F 3212/ MT-R 3319, table 3), and 4 µl of treated or non-treated DNA. Samples were run in triplicate by 7900HT Fast Real-Time PCR System (Applied Biosystems, Foster City, CA, USA) with following thermal cycling profile: 5 min at 95°C and 35 cycles of 15 sec at 95° C plus 1 min at 60°C. Afterwards, differences in amplification efficiency between non-treated and treated DNA (ΔCt) were calculated. The ΔCt is proportional to 8OHdG content and it represents the oxidative damage.

mtDNA CN quantification

Mitochondrial DNA Copy Number (mtDNA CN) was measured using RT-PCR assay by determining the ratio of mitochondrial gene copy number (*MT-ND1*- subunit of NADH dehydrogenase,) to single-copy nuclear control genes, human beta globin (*Hbg*).

For each plate a control standard curve (range 80-0.33 ng/µL of "DNA pool") was done. Isolated genomic DNA (12.5 ng) was added to 7.5 µl master mix consisting of Fast SYBR® Green I dye 2× (5 µl/reaction), forward and reverse primer (each 0.3 µl/reaction) and RNase free water (1.9 µl/reaction), for a final volume of 10 µl per reaction. Primers (MT-F 3212 / MT-R 3319) were diluted to a final concentration of 500 nM in the master mix. The samples were run in triplicate, in 384-well format, using the 7900HT Fast Real-Time PCR with thermal cycling profile described in table 3.

Telomere Length quantification

Telomere Length was measured using RT-PCR assay by determining the ratio (T/S) of the telomere repeat copy number (T) to single-copy nuclear control genes (S), human beta globin (*Hbg*). For each plate a control standard curve (range 80-0.33 ng/µL of "DNA pool") was done. Isolated genomic DNA (12.5 ng) was added to 7 µl master mix consisting of Fast SYBR® Green I dye 2× (5 µl/reaction), forward and reverse primer (each 0.4 µl/reaction) and RNase free water (1.2 µl/reaction), for a final volume of 10 µl reaction. Primers (TEL C, TEL G) were diluted to a final concentration of 400 nM in the master mix. The samples were run in triplicate, in 384-well format, using the 7900HT Fast Real-Time PCR System with thermal cycling profile described in table 3.

Table 3. Primers and thermic profile conditions

Sequence ID	Primers	Thermic profiling
TEL G	5-ACACTAAGGTTTGGGTTTGGGTTTGGGTTTGGGTTAGTGT-3	**2 cycles with:** 50 °C for 2' 95 °C for 2' 95 °C for 15'' 49 °C for 1' **35 cycles with:** 95 °C for 15'' 62 °C for 10'' 74 °C for 15''
TEL C	5-GTTAGGTATCCCTATCCCTATCCCTATCCCTATCCCTAACA-3	
MT-F 3212	5-CACCCAAGAACAGGGTTTGT-3	50 °C for 2' 98 °C for 3' **35 cycles with:** 95 °C for 15'' 60 °C for 1'
MT-R 3319	5-TGGCCATGGGTATGTTGTTA-3	
Hbg F	5-GCTTCTGACACAACTGTGTTCACTAGC-3	50 °C for 2' 95 °C for 2' **35 cycles with:** 95 °C for 15'' 58 °C for 1'
Hbg R	5-CACCAACTTCATCCACGTTCACC-3	

HERV-w and EBV methylation analysis

Bisulfite treatment

Sodium bisulfite DNA treatment allows for discrimination between methylated and unmethylated cytosines: unmethylated cytosines are deaminated to uracil, while 5-methyl-cytosines (5mC) are resistant to conversion. During PCR reaction, uracils are replaced by thymines, while methylated cytosines remain as cytosines and can be differentiated from the unmethylated ones.

Briefly, 20 µl of DNA (concentration 25 ng/µl) was treated using EZ DNA Methylation-Gold kit (Zymo Research, Orange, Ca, USA) according to the manufacturer's instructions. Final elution was performed with 30 µl M-Elution Buffer. The samples were the dilute in 300 µl with ultrapure water.

Polymerase chain reaction

The polymerase chain reaction (PCR) is a technique used to amplify a single or a few copies of a DNA, generating thousands to millions of copies of a particular DNA sequence. The assays for HERV-w (Human chromosome 17, sequence 92098183-92098402), Wp-EBV (viral genome, sequence 17286-17445) and Cp-EBV (sequence 11170-1286) methylation, were designed using PSQ assay design software (Qiagen). Briefly, 50 µL PCR reaction was carried out with 25 µL of Hot Start GoTaq Green Master mix (Promega), 1 pmol of forward primer, 1 pmol of reverse primer and 25 ng of bisulfite-treated genomic DNA.

HERV-w and EBV Primers and PCR cycling conditions are resumed in table 4.

Table 4. Primers and PCR conditions used in HERV-w and EBV methylation study

Sequence ID	Primers	Sequence analysed	PCR conditions
HERV-w	F: -ATGGAGTTTAAGATGTAGTTTAAG- R: bio -CAATCCCCCATCTCAACAA- S: -AGTTTAAGATTAAGATTTAT-	C/TGTAGATTTTTGGATC/TGGTTTGTTAGTT TAC/TGATTT	95 °C for 5' 95 °C for 1' 55 °C for 1' 72 °C for 1' 72 °C for 5' **50 cycles**
EBV-Cp	F: bio- GAGGGGAAAAGAGGAATAAGTTTT- R: -CCCCTCCCTAAAACTAACAATTAAC- S: -CAATTAACTACTATCTAACT-	TACA/GTAAACA/GCA/GCTAAACTAAAAAA ATAACCTAACAACA/GCA/GAACCCCCTT	95 °C for 5' 95 °C for 1' 51 °C for 1' 72 °C for 1' 72 °C for 10' **45 cycles**
EBV-Wp	F: bio- GTTTAAAGTGGTAATAATATTAGG- R: -AACTCCATTTTTCAAATC- S: -AACTCCATTTTTCAAATC-	A/GTAAACA/GAATTAACTAAACTTACA/GT AAACAAAACA/GTAATT	95 °C for 5' 95 °C for 1' 45 °C for 1' 72 °C for 1' 72 °C for 10' **45 cycles**

F: forward primer, R: reverse primer, S: sequencing primer

Pyrosequencing

Pyrosequencing is based on the "sequencing by synthesis" method: a single strand DNA is sequenced by the synthesis of the complementary strand.

In a cascade of enzymatic reactions, visible light is generated proportionally to the number of incorporated nucleotides, according to the sequence of the template (figure 15). Although a wide variety of different methods are available, pyrosequencing is the only one that permits an accurate quantification for every single C site and a very low intra-run variability, which is necessary to study healthy tissue exposed to environmental pollutants. Biotin-labelled primers were used to purify the final PCR product with Sepharose HP beads (Amersham Biosciences, Uppsala, Sweden). The purified PCR product was then washed, denatured with 0.2 M NaOH, and washed again with the Pyrosequencing Vacuum Prep Tool (Pyrosequencing, Inc., Westborough, MA, USA), according to the manufacturer's instructions, and sequenced using 0.3 μM sequencing primer. The methylation level at CpG positions within each gene's promoter region, was expressed as the percentage of methylated cytosines determined as the number of methylated cytosines divided by the sum of methylated and unmethylated cytosines. Every sample was tested two times for each marker to confirm reproducibility and to increase the precision.

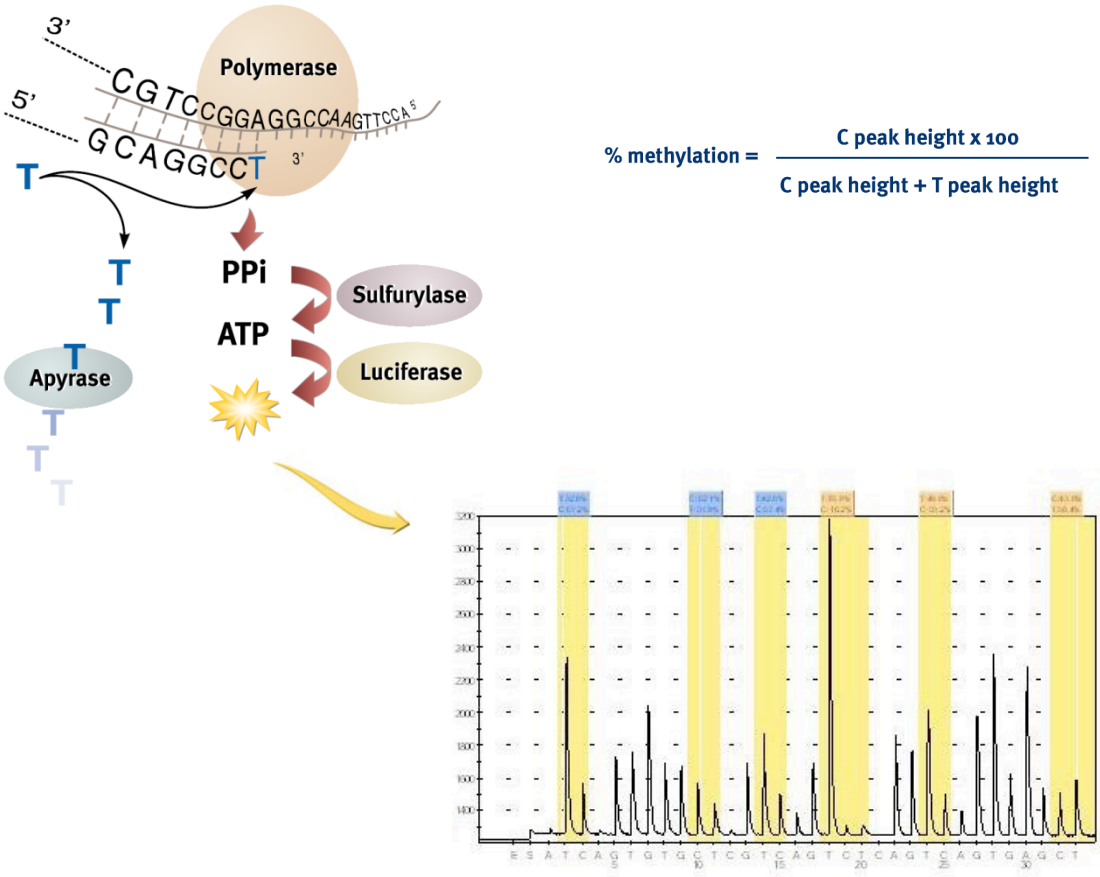

Figure 15. Pyrosequencing principle

Statistical analysis

Descriptive statistics were performed on all variables. Continuous data were expressed as mean ± SD or as median [Q1; Q3] if not normally distributed. Categorical variables are presented as absolute numbers and frequencies.

Oxidative stress markers

We evaluated the association of the levels of PM (PM_{10} and $PM_{2.5}$ from Day -1 to Day -7) with telomere length, 8OHdG and mitochondrial DNA using multivariable linear regression models. Telomere length was log-transformed (base e) to achieve normal distribution. All effects were reported as percent change (Δ%) with 95% confidence interval (95% CI), which corresponds to the percent increase in oxidative stress markers for 10 $\mu g/m^3$ increase in PM concentration. We also applying multiple linear regression models to evaluate the association of telomere length with 8-OHdG and mitochondrial DNA.

DNA Methylation markers

DNA methylation measurements for each subject were performed for more CpG dinucleotide positions (three for HERV-w methylation and five for EBV-Wp methylation) replicated in two measurements. To consider intra-individual correlation due to repeated-measure data structure we designed linear mixed models. The CpG dinucleotide position was considered introducing a random effect model. We evaluated the association of exposure (PM_{10} and $PM_{2.5}$ from Day -1 to Day -7) with HERV-w and EBV-Wp methylation. Methylation markers were naturally log-transformed to approximately normal distributions. Effects were reported as

percent change (Δ%) with 95% confidence interval (95% CI), which corresponds to the percent increase in DNA methylation markers for 10 μg/m^3 increase in PM concentration.

All linear regression models were adjusted for age, gender, BMI and smoking habits (categories: never, former, and current smoker). For each linear regression model, we evaluate the possible effect modification of BMI, subjects were stratified according to the standard CDC definition of overweight subjects (BMI < or ≥25 kg/m^2) and two separate linear regression models (adjusted for age, gender and smoking habits) were run.

Interaction was tested by adding an interaction term (BMI x PM exposure) to each multivariate regression model.

We checked regression assumptions by performing diagnostic tests for each model. A two-sided p-value < 0.05 was considered statistically significant.

Data analysis was performed using SAS (version 9.4; SAS Institute Inc., Cary, NC, USA).

RESULTS

Study subjects characteristics

The characteristics of the study participants are summarized in table 5. The population included 50 healthy subjects (20 males and 30 females). The mean age was 48.4 (± 8.3) years. 27 subjects had normal weight (BMI ≤25; 54%) and 23 were overweight (BMI >25; 46%). Half of the study participants were no smoker (56%), most were employed (94%) and had completed university (62%). The majority of this population lived in the city or province of Milan and worked in the city of Milan (84%).

Table 5. Demographic and lifestyle characteristics of study participants (N=50)

CHARACTERISTICS	N (%)
Age, years *(mean ± SD)*	48.4 ± 8.3
Sex	
Male	20 (40%)
Female	30 (60%)
BMI, Kg/m^2 *(mean ± SD)*	24.3 ± 3.2
<25 normal weight	27 (54%)
≥25 overweight	23 (46%)
Smoking habits	
Never smoker	28 (56%)
Ex-smoker	13 (26%)
Current smoker	9 (18%)
Education	
Primary school or less	-
Secondary school	-
High school	13 (26%)
University	31 (62%)
Others	6 (12%)
Occupation	
Currently employed	47 (94%)
Retired	3 (6%)
Living area	
City of Milan	24 (48%)
Province of Milan	13 (26%)
Province of Monza-Brianza	7 (14%)
Others province in Lombardy	6 (12%)
Work area	
City of Milan	42 (84%)
Province of Milan	2 (4%)
Province of Monza-Brianza	2 (4%)
Province of Como	1 (2%)

PM_{10} and $PM_{2.5}$ exposure in study

Figure 16 reports box plots summarizing PM_{10} and $PM_{2.5}$ concentrations at different days preceding date of recruitment (Day -1 to Day -7), measured by Personal Cascade Impactor Samplers (PCIS, only for Day -1) and Monitoring Stations (MS) or estimated by Chemical Transport Model (CTM), according to the methods described in material and methods.

In the 7 days, preceding blood drawing, the median PM_{10} and $PM_{2.5}$ concentrations ranged respectively from 41 to 57 and from 32 to 43 μg/m^3).

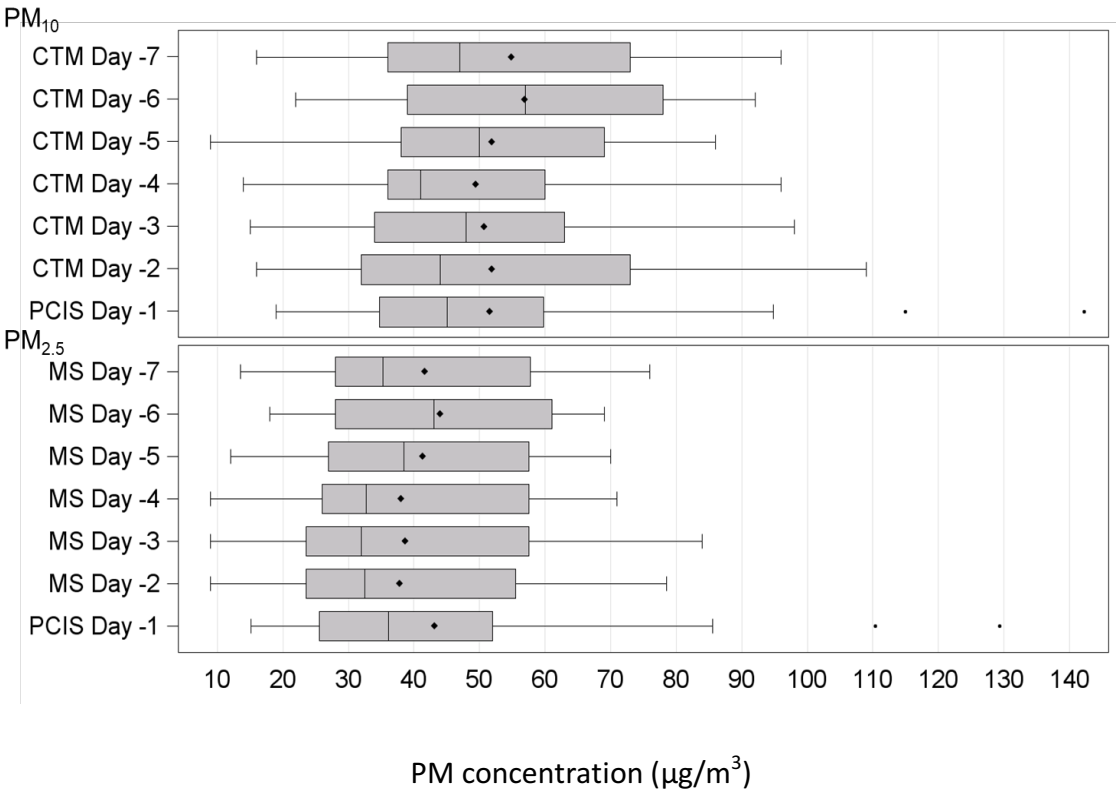

Figure 16. Box plots summarizing PM_{10} and $PM_{2.5}$ concentrations at different days preceding date of recruitment (Day -1 to Day -7), measured by Personal Cascade Impactor Samplers (PCIS), Monitoring Stations (MS) or estimated by Chemical Transport Model (CTM)

Association between PM exposure and markers

8OHdG and PM exposure association

Table 6 shows the associations of mitochondrial 8OHdG with the levels of personal PM_{10} and $PM_{2.5}$ (Day -1), and with the levels of ambient PM_{10} and $PM_{2.5}$ (from Day -2 to Day -7). We expressed all results as percent changes in 8OHdG associated with an increase equal to 10 $\mu g/m^3$ in the exposure variable. All results are adjusted by age, gender and smoking habits.

Considering the entire study population, mitochondrial 8OHdG levels were negatively associated with PM_{10} and $PM_{2.5}$ exposure measured 3, 5, 6 and 7 days before blood drawing.

The maximum effect was observed for $PM_{2.5}$ measured at Day -5, which was associated with a -28.69% (95% CI: -45.32; -12.07) decrease in 8OHdG levels (p=0.0016) (as also shown in figure 17).

Taking into accounts previous findings in this population that showed BMI as an effect modifier of the relationship between PM exposure and extracellular vesicles [107], we decided to stratify according to BMI (<25 or ≥25). Even if the p-value for interaction was not statistically significant, the observed effect was more visible in the overweight subjects (table 6).

		All subjects (N=50)				BMI < 25 (N=27)				BMI ≥ 25 (N=23)				P-value for
		Δ%*	95% CI		P-value	Δ%*	95% CI		P-value	Δ%*	95% CI		P-value	interaction
8OHdG	**PM_{10} exposure**													
	Day -1	-7.80	-20.76	5.16	0.2448	-1.31	-21.50	18.88	0.8998	-12.86	-29.97	4.25	0.1312	0.4201
	Day -2	-12.03	-25.96	1.90	0.0977	-0.43	-17.46	16.61	0.9611	-16.18	**-32.00**	-0.35	**0.0456**	0.4974
	Day -3	**-19.07**	-32.73	-5.40	**0.0089**	-12.30	-26.72	2.12	0.1094	-20.24	-41.31	0.84	0.0588	0.6167
	Day -4	-13.89	-28.51	0.73	0.0693	-9.52	-24.09	5.06	0.2146	-14.15	-38.88	10.58	0.2449	0.6353
	Day -5	**-19.32**	-32.98	-5.67	**0.0081**	-9.03	-22.63	4.56	0.2069	-27.89	**-49.23**	-6.56	**0.0133**	0.7639
	Day -6	**-20.76**	-33.83	-7.69	**0.0032**	-8.47	-23.49	6.54	0.2810	-30.93	**-47.62**	-14.25	**0.0011**	0.2602
	Day -7	**-18.98**	-31.03	-6.93	**0.0035**	-9.42	-24.12	5.28	0.2229	-27.21	**-41.40**	-13.02	**0.0008**	0.2628
	$PM_{2.5}$ exposure													
	Day -1	-10.46	-24.36	3.43	0.1473	-5.93	-25.28	13.42	0.5543	-14.37	-33.34	4.60	0.1283	0.7066
	Day -2	-13.15	-29.97	3.67	0.1326	-2.37	-22.33	17.60	0.8185	-17.76	-38.22	2.71	0.0850	0.6778
	Day -3	**-19.36**	-34.39	-4.33	**0.0152**	-10.74	-24.88	3.41	0.1517	-26.75	-53.54	0.04	0.0503	0.4854
	Day -4	-11.61	-28.33	5.12	0.1809	-8.52	-25.69	8.65	0.3424	-11.30	-38.33	15.74	0.3915	0.4865
	Day -5	**-28.69**	-45.32	-12.07	**0.0016**	-15.25	-31.65	1.16	0.0843	-38.98	**-64.32**	-13.63	**0.0046**	0.4840
	Day -6	**-25.53**	-41.92	-9.14	**0.0039**	-13.00	-31.87	5.87	0.1920	-35.19	**-57.05**	-13.33	**0.0033**	0.4975
	Day -7	**-20.62**	-36.80	-4.44	**0.0166**	-13.51	-32.88	5.85	0.1873	-36.77	**-59.49**	-14.04	**0.0033**	0.5335

* $\Delta\% = (1-((Y_{min} - \beta)/Y_{min})) * 100$, percent increase in 8OHdG for 10 $\mu g/m^3$ increase in PM concentration. Association between 8OHdG and PM exposure in all subjects. Results from a multivariable regression models adjusted for age, gender, BMI and smoking habit (never, former, current smoker).
Association between 8OHdG and PM exposure, stratifying subjects by BMI (< vs ≥25 kg/m^2). Results from a multivariable regression models adjusted for age, gender and smoking habit (never, former, current smoker).

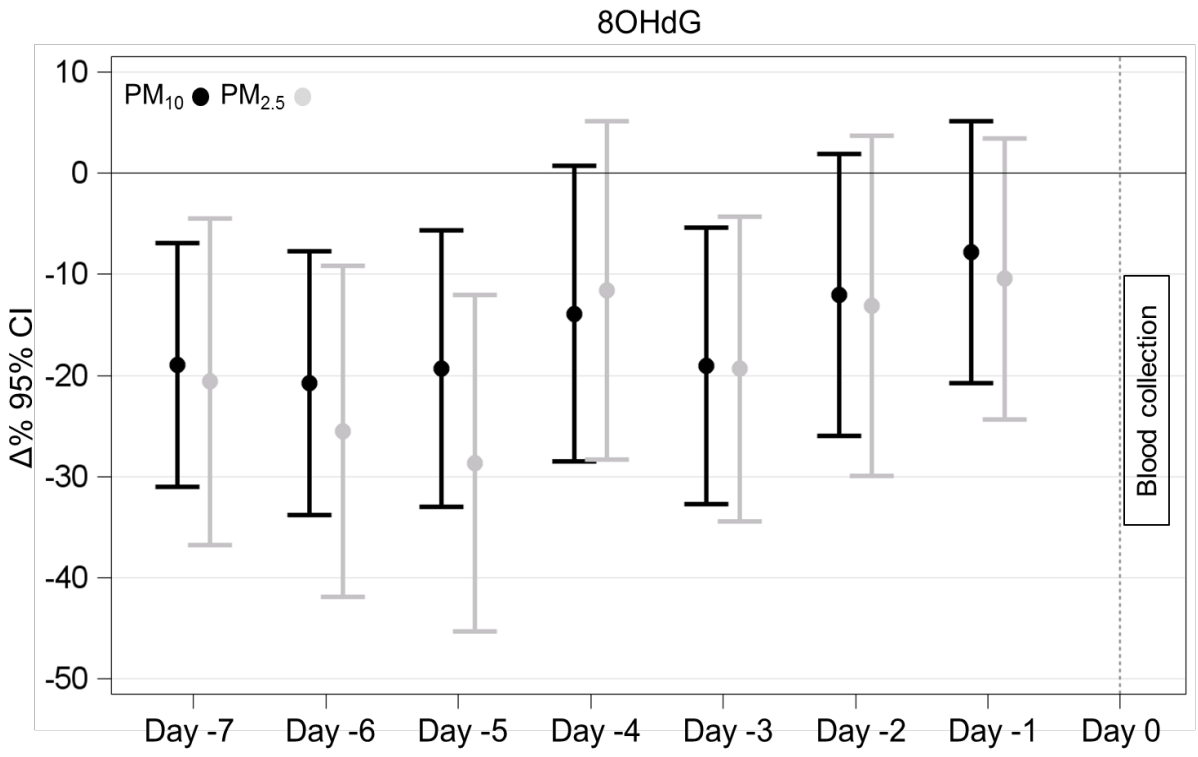

Figure 17. Association between 8OHdG and PM_{10} / $PM_{2.5}$ exposures measured at different time lags (from one day before date of blood drawing (Day -1) to Day -7). Linear regression models were adjusted for age, gender, BMI and smoking habit (never, former, current). Δ% is equal to $(1- ((Y_{Min} – \beta*10)/Y_{Min})) * 100$ and represents the percent increase in 8OHdG for 10 µg/m^3 increase in PM concentration. Y_{Min} is the minimum value observed of 8OHdG

Association between mtDNA CN and PM exposure

The associations between PM_{10}/$PM_{2.5}$ exposure and mitochondrial copy number are reported in table 7 and figure 18.

In either normal and overweight subjects, we did not observe any effect of PM_{10} / $PM_{2.5}$ exposure on DNA mitochondrial copy number. The result was also confirmed after stratifying by BMI.

Table 7. Association between mitochondrial DNA and PM exposure

		All subjects (N=50)				BMI < 25 (N=27)				BMI ≥ 25 (N=23)				P-value for
		Δ%*	95% CI		P-value	Δ%*	95% CI		P-value	Δ%*	95% CI		P-value	interaction
Mitochondrial DNA	**PM_{10} exposure**													
	Day -1	0.02	-5.16	5.20	0.9946	2.65	-9.84	15.14	0.6817	-0.53	-5.47	4.41	0.8364	0.4945
	Day -2	-4.88	-10.37	0.61	0.0884	-6.73	-16.91	3.44	0.2087	-3.98	-8.43	0.48	0.0970	0.8901
	Day -3	-0.39	-6.22	5.45	0.8975	3.12	-6.32	12.55	0.5242	-5.31	-11.16	0.53	0.0916	0.2465
	Day -4	-2.00	-7.96	3.97	0.5149	-1.75	-11.11	7.61	0.7178	-1.66	-8.60	5.28	0.6455	0.8936
	Day -5	-3.00	-8.78	2.77	0.3136	-0.67	-9.44	8.10	0.8821	-3.38	-10.10	3.35	0.3383	0.7592
	Day -6	-4.23	-9.79	1.33	0.1432	-2.37	-11.90	7.16	0.6307	-3.32	-9.28	2.64	0.2897	0.6819
	Day -7	-2.82	-8.00	2.36	0.2921	-0.45	-9.91	9.01	0.9265	-2.14	-7.36	3.08	0.4328	0.8840
	$PM_{2.5}$ exposure													
	Day -1	0.52	-5.08	6.12	0.8558	3.77	-8.23	15.78	0.5446	-0.68	-6.16	4.80	0.8099	0.5855
	Day -2	-6.20	-12.76	0.36	0.0707	-7.48	-19.47	4.51	0.2348	-5.54	-11.03	0.06	0.0631	0.9752
	Day -3	0.05	-6.30	6.39	0.9888	2.23	-6.95	11.41	0.6389	-5.92	-13.56	1.73	0.1467	0.2538
	Day -4	-3.61	-10.31	3.09	0.2966	-3.15	-14.11	7.81	0.5793	-1.73	-9.19	5.72	0.6539	0.9205
	Day -5	-2.08	-9.12	4.97	0.5661	3.40	-6.84	13.64	0.5225	-5.37	-13.66	2.92	0.2207	0.3950
	Day -6	-4.54	-11.59	2.52	0.2143	-2.00	-14.36	10.36	0.7544	-2.89	-10.37	4.59	0.4585	0.6550
	Day -7	-5.70	-12.32	0.91	0.0986	-5.25	-17.53	7.02	0.4118	-3.78	-11.50	3.93	0.3498	0.7359

* $\Delta\% = (1-((Y_{min} - \beta)/Y_{min})) * 100$, percent increase in mitochondrial DNA for 10 $\mu g/m^3$ increase in PM concentration. Association between mtDNA CN and PM exposure in all subjects. Results from a multivariable regression models adjusted for age, gender, BMI and smoking habit (never, former, current smoker). Association between mtDNA CN and PM exposure, stratifying subjects by BMI (< vs ≥25 kg/m^2). Results from a multivariable regression models adjusted for age, gender and smoking habit (never, former, current smoker).

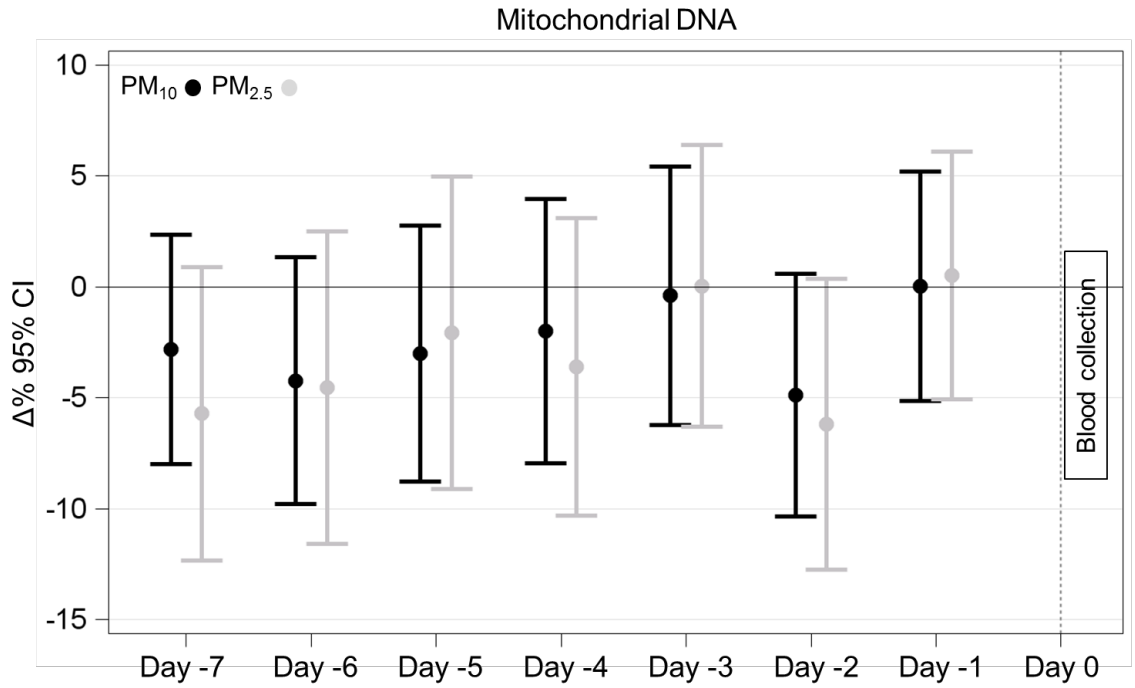

Figure 18. Association between mitochondrial DNA CN and PM_{10} / $PM_{2.5}$ exposures measured at different time lags (from one day before date of blood drawing (Day -1) to Day -7). Linear regression models were adjusted for age, gender, BMI and smoking habit (never, former, current). Δ% is equal to $(1- ((Y_{Min} – \beta*10)/Y_{Min})) * 100$ and represents the percent increase in mitochondrial DNA for $10\mu g/m^3$ increase in PM concentration. Y_{Min} is the minimum value observed of mitochondrial DNA CN

TL and PM exposure

Table 8 shows the associations of TL with the levels of personal PM_{10} and $PM_{2.5}$ (Day -1), and with the levels of ambient PM_{10} and $PM_{2.5}$ (from Day -2 to Day -7). We expressed all results as percent changes in TL associated with an increase equal to 10 $\mu g/m^3$ in the exposure variable. All results are adjusted by age, gender and smoking habits. In all subjects, personal PM_{10} exposure at Day -2 was associated with a 4.2% (95% CI: 0.45; 8.09) increase in TL (p=0.0331).

After stratifying the population according to their BMI (<25 or ≥25), we observed a different effect in overweight subjects, compared to normal weight subjects, which was maximum at Day -5. In particular, in normal weight subjects, PM_{10} and $PM_{2.5}$ were both not significantly associated with TL. On the contrary, in overweight subjects we found that increased levels of PM_{10} and $PM_{2.5}$ were associated with increased TL at several time lags (PM_{10} measured 2, 3, 5, 6 and 7 days before blood drawing and $PM_{2.5}$ measured 3 and 5 days before blood drawing). The maximum effect was observed for $PM_{2.5}$ measured at Day -5, which was associated with a 9.25% (95% CI: 2.16; 16.82) increase in TL (p=0.0039) (figure 19).

Table 8. Association between telomere length and PM exposure.

		All subjects (N=50)				BMI < 25 (N=27)				BMI ≥ 25 (N=23)				P-value for interaction
		Δ%*	95% CI		P-value	Δ%*	95% CI		P-value	Δ%*	95% CI		P-value	
Telomere Lenght	**PM_{10} exposure**													
	Day -1	2.07	-1.41	5.67	0.2542	0.46	-6.59	8.04	0.9034	2.75	-1.60	7.30	0.2352	0.5499
	Day -2	**4.20**	**0.45**	**8.09**	**0.0331**	1.44	-4.57	7.83	0.6515	**4.22**	**0.21**	**8.40**	**0.0539**	0.5992
	Day -3	2.70	-1.22	6.77	0.1865	-0.30	-5.66	5.37	0.9172	**5.70**	**0.40**	**11.29**	**0.0489**	**0.0404**
	Day -4	0.25	-3.76	4.42	0.9059	-1.11	-6.34	4.41	0.6917	3.10	-3.07	9.67	0.3450	0.3907
	Day -5	2.49	-1.44	6.57	0.2244	-0.30	-5.25	4.91	0.9100	**7.21**	**1.60**	**13.13**	**0.0206**	**0.0040**
	Day -6	1.93	-1.91	5.91	0.3347	0.93	-4.52	6.70	0.7457	**5.55**	**0.41**	**10.96**	**0.0480**	0.1174
	Day -7	1.94	-1.59	5.60	0.2904	0.92	-4.46	6.61	0.7455	**5.32**	**1.01**	**9.82**	**0.0258**	0.0523
	$PM_{2.5}$ exposure													
	Day -1	2.28	-1.49	6.19	0.2456	0.27	-6.54	7.57	0.9414	2.95	-1.89	8.03	0.2527	0.4624
	Day -2	3.39	-1.19	8.18	0.1563	-0.02	-6.97	7.45	0.9960	4.27	-0.95	9.77	0.1277	0.5772
	Day -3	2.81	-1.46	7.26	0.2069	-0.24	-5.45	5.25	0.9299	**7.66**	**0.85**	**14.92**	**0.0400**	**0.0098**
	Day -4	-0.30	-4.75	4.37	0.8993	-0.56	-6.59	5.85	0.8611	2.31	-4.34	9.42	0.5135	0.4531
	Day -5	2.74	-2.27	8.01	0.2956	-0.28	-6.53	6.38	0.9322	**9.25**	**2.16**	**16.82**	**0.0186**	**0.0039**
	Day -6	1.07	-3.70	6.07	0.6690	0.77	-6.05	8.09	0.8314	5.33	-1.26	12.36	0.1324	0.1765
	Day -7	0.60	-3.99	5.40	0.8043	0.47	-6.52	7.99	0.8994	6.70	-0.10	13.96	0.0706	0.0900

* Δ% = (exp (β*10) -1) *100, percent increase in telomere length for 10 μg/m^3 increase in PM concentration. Association between telomere length and PM exposure in all subjects. Results from a multivariable regression models adjusted for age, gender, BMI and smoking habit (never, former, current smoker).

Association between telomere length and PM exposure, stratifying subjects by BMI (< vs ≥ 25 kg/m^2). Results from a multivariable regression models adjusted for age, gender and smoking habit (never, former, current smoker).

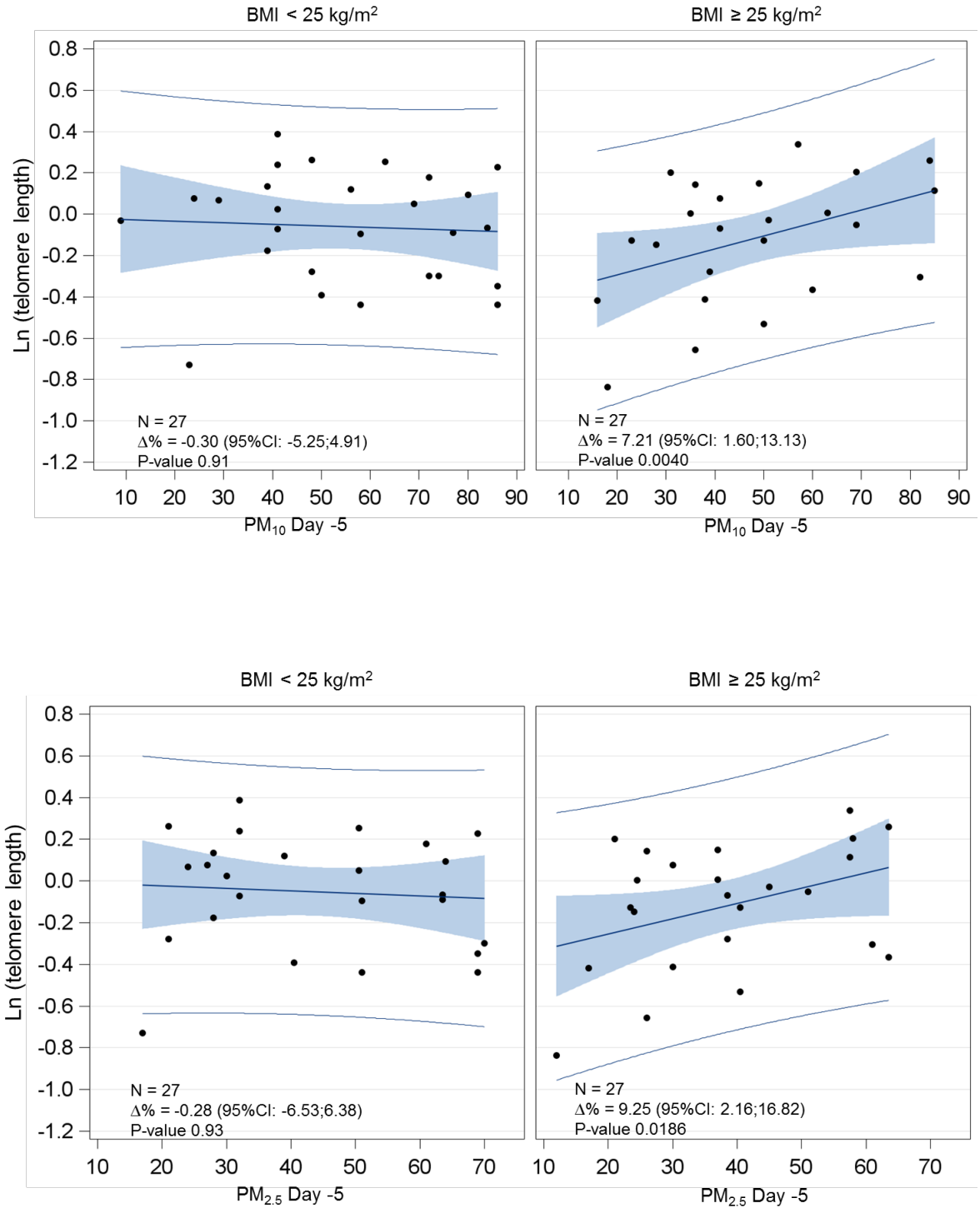

Figure 19. Association between telomere length and individual Day -5 PM_{10}/$PM_{2.5}$ exposure. Scatterplots of telomere length after natural logarithmic transformation versus PM_{10} (*above*) or $PM_{2.5}$ (*below*) levels (μg/m^3), in subjects with BMI <25 (*left*) or ≥25 (*right*) kg/m^2. Covariate-adjusted Δ% and corresponding 95% Confidence Intervals Δ% (95%CI) in telomere length estimated per 10-unit increase in PM are shown. Linear regression models reported in all panels were adjusted for age, gender and smoking habit

Association between TL and mtDNA CN or 8OHdG

Oxidative stress levels have been consistently inversely associated with telomere length, as a higher oxidative stress increases telomere attrition [110].

We therefore examined the relationship between telomere length and mtDNA CN or 8OHdG (table 9).

In the whole study population, we observed a significant decrease -19.87% (95%CI: -34.27; -2.31) in telomere length for each 1-unit increase in 8OHdG (P-value=0.0293) (figure 20), while no association between mtDNA CN and telomere length was found.

After BMI stratification, the relation between telomere length increase and 8OHdG was confirmed only in overweight subjects (-39.10%; 95%CI: -51.54; -23.47; p-value=0.0002) (figure 21).

In addition, a negative relationship between mtDNA CN and telomere length was also observed in overweight subjects only as shown in figure 22-23.

Table 9. Association between telomere length and 8OHdG / mitochondrial DNA

TL	All subjects (N=50)				BMI < 25 (N=27)				BMI ≥ 25 (N=23)				P-value for interaction
	Δ%*	95% CI		P-value	Δ%*	95% CI		P-value	Δ%*	95% CI		P-value	
8OHdG	**-19.87**	**-34.27**	**-2.31**	**0.0293**	-2.6	-25.82	27.88	0.8424	**-39.1**	**-51.54**	**-23.47**	**0.0002**	**0.0318**
mtDNA CN	21.65	-16.67	77.58	0.3022	30.75	-18.48	109.72	0.2511	-22.67	-62.1	57.81	0.4588	**0.0174**

* Δ% = (exp (β) -1) * 100, percent increase in telomere length for 1-unit increase in 8OHdG/ mitochondrial DNA CN. Association between telomere length and 8OHdG/ mitochondrial DNA CN in all subjects. Results from a multivariable regression models adjusted for age, gender, BMI and smoking habit (never, former, current smoker). Association between telomere length and 8OHdG/ mitochondrial DNA CN, stratifying subjects by BMI (< vs ≥25 kg/m^2). Results from a multivariable regression models adjusted for age, gender and smoking habit (never, former, current smoker).

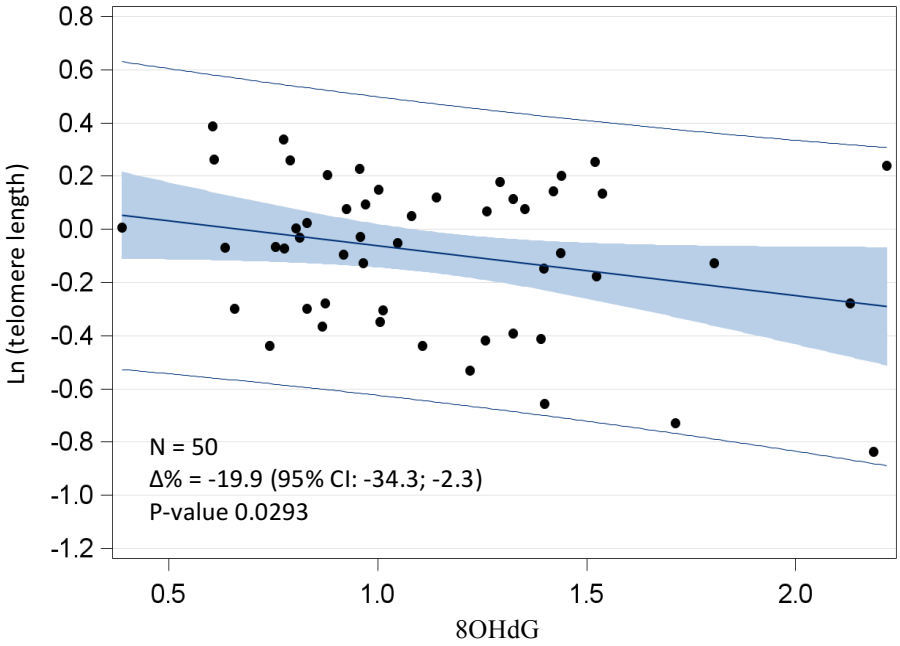

Figure 20. Association of telomere length and 8OHdG. Scatterplot of telomere length after natural logarithmic transformation versus 8OHdG. Covariate-adjusted Δ% and 95% Confidence Intervals Δ% (95% CI) in telomere length estimated per 1-unit increase in 8OHdG are shown. Linear regression model reported was adjusted for age, gender, BMI and smoking habit

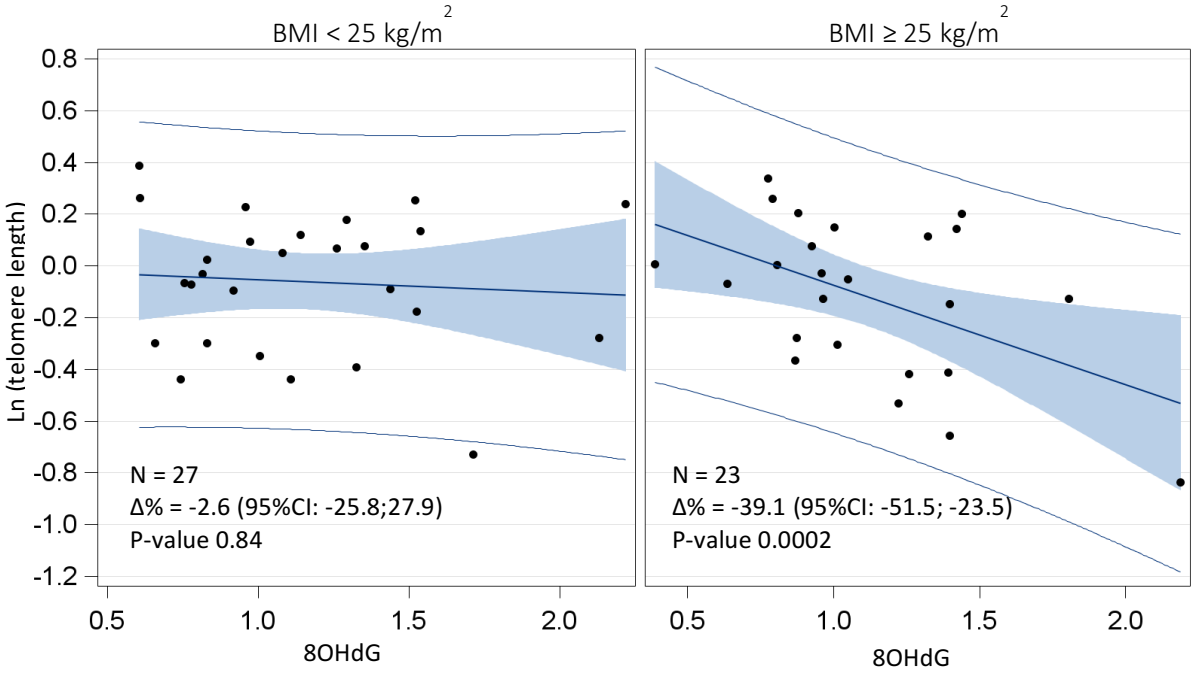

Figure 21. Association of telomere length and 8OHdG. Scatterplots of telomere length after natural logarithmic transformation versus 8OHdG, in subjects with BMI <25 (*left*) or ≥25 (*right*) kg/m^2. Covariate-adjusted Δ% and 95% Confidence Intervals [Δ% (95%CI)] in telomere length estimated per 1-unit increase in 8OHdG are shown. Linear regression models reported were adjusted for age, gender and smoking habit

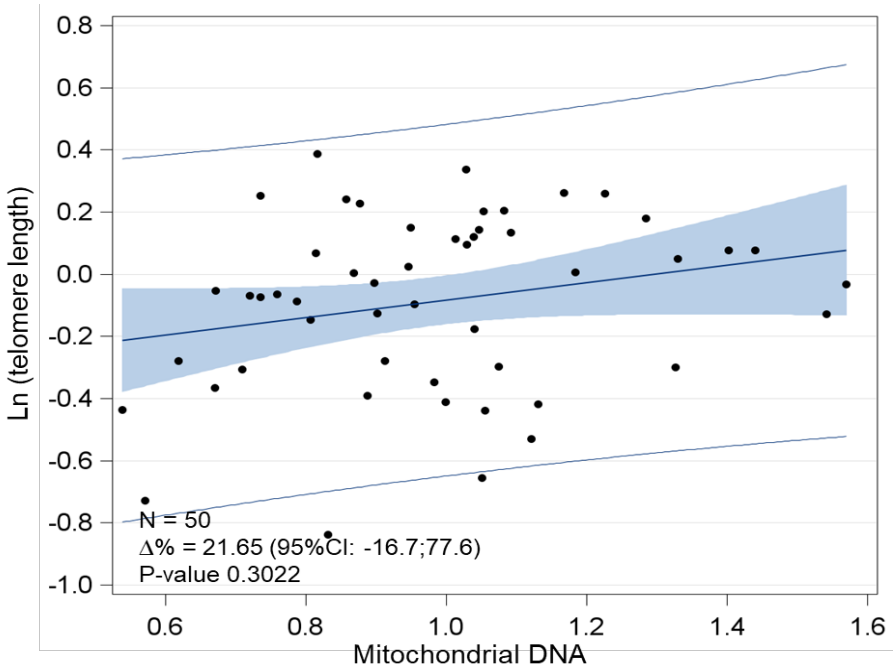

Figure 22. Association of telomere length and mitochondrial DNA CN. Scatterplot of telomere length after natural logarithmic transformation versus mitochondrial DNA. Covariate-adjusted Δ% and 95% Confidence Intervals Δ% (95% CI) in telomere length estimated per 1-unit increase in mitochondrial DNA are shown. Linear regression model reported was adjusted for age, gender, BMI and smoking habit

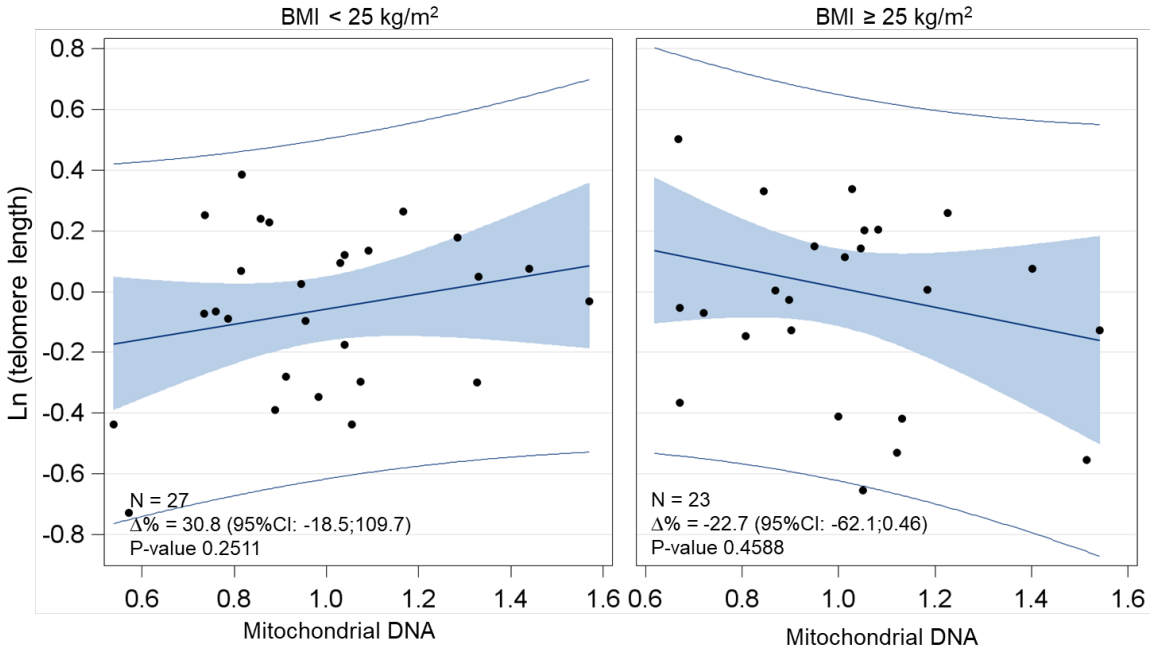

Figure 23. Association of telomere length and mitochondrial DNA CN. Scatterplots of telomere length after natural logarithmic transformation versus mitochondrial DNA, in subjects with BMI <25 (*left*) or ≥25 (*right)* kg/m^2. Covariate-adjusted Δ% and 95% Confidence Intervals Δ% (95% CI)] in telomere length estimated per 1-unit increase in mitochondrial DNA CN are shown. Linear regression models reported were adjusted for age, gender and smoking habit

Association between EBV and HERV-w virus DNA methylation and PM exposure

PM exposure has been related to systemic changes in DNA methylation. In addition, global hypomethylation, frequently related to PM exposure, has been associated to viral sequence reactivation, possibly linked to the activation of pro-inflammatory pathways occurring after exposure. This observation provided a rationale to investigate both exogenous (EBV) and endogenous (HERV-w) viral sequence methylation in association to PM exposure. Figure 24 reports a description of EBV and HERV-w methylation. 5 CpG positions were considered within EBV promoter, and 3 position in the HERV-w promoter and individual levels of methylation are reported.

Percent increases in of EBV and HERV-w DNA methylation for each 10 $\mu g/m^3$ increase in PM concentrations are shown in table 9 and figure 25-26.

After adjustments for age, gender, BMI and smoking habits, HERV-w methylation levels were negatively associated with PM_{10} and $PM_{2.5}$ exposure measured 3 days before blood drawing (respectively -0.10%; 95% CI: -0.19; -0.01; p-value=0.0326 and -0.11%; 95% CI: -0.20; -0.01; p-value=0.0371).

We also observed a strong negative effect of both PM_{10} and $PM_{2.5}$ exposure measured 4, 5 and 6 days before blood drawing on EBV-Wp methylation (table 9).

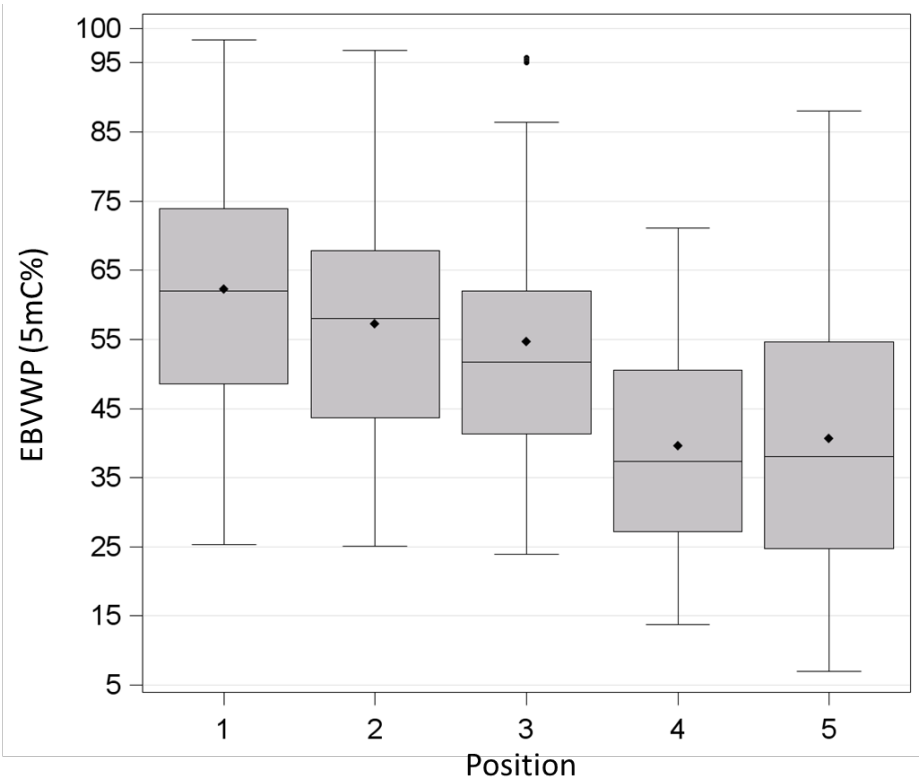

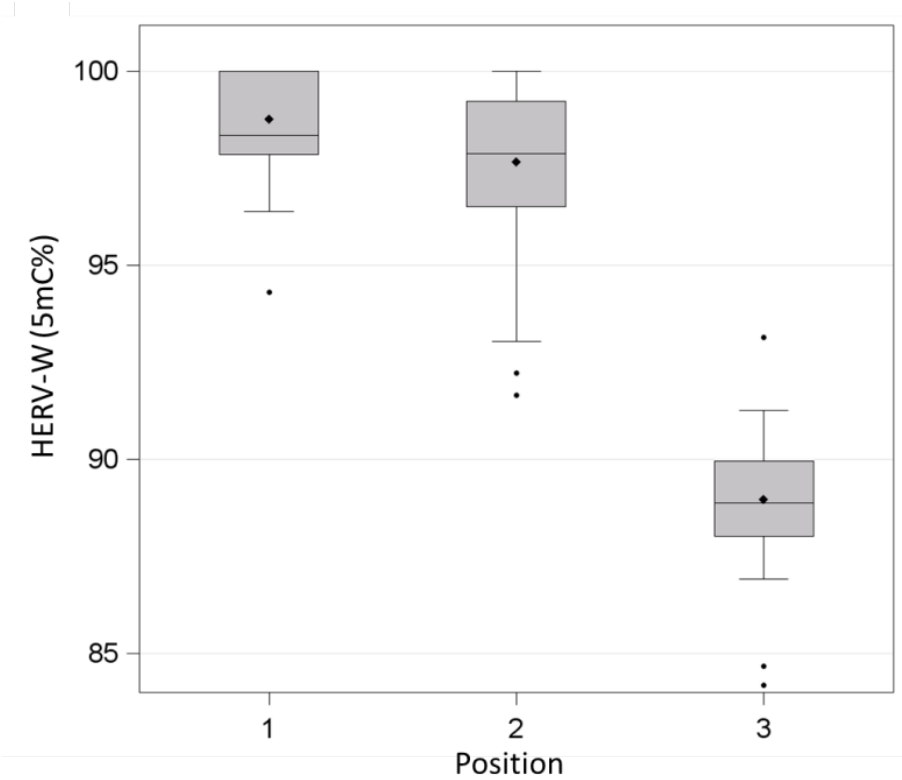

Figure 24. Descriptive statistics of DNA EBV/HERV-w methylation markers in all subjects (N=50)

Table 9. Association between DNA methylation markers and PM exposure

		All subjects (N=50)			
		Δ%*	95% CI		P-value
HERV-w	PM_{10} exposure				
	Day -1	0.01	-0.07	0.09	0.8850
	Day -2	0.01	-0.08	0.09	0.9065
	Day -3	**-0.10**	**-0.19**	**-0.01**	**0.0326**
	Day -4	-0.05	-0.14	0.05	0.3158
	Day -5	0.04	-0.06	0.13	0.4592
	Day -6	0.01	-0.08	0.10	0.8557
	Day -7	0.02	-0.07	0.10	0.6714
	$PM_{2.5}$ exposure				
	Day -1	0.003	-0.08	0.09	0.9387
	Day -2	-0.03	-0.14	0.08	0.5985
	Day -3	**-0.11**	**-0.20**	**-0.01**	**0.0371**
	Day -4	-0.04	-0.15	0.07	0.4570
	Day -5	0.01	-0.11	0.13	0.9039
	Day -6	-0.03	-0.15	0.08	0.5793
	Day -7	-0.03	-0.14	0.08	0.6251
EBV-Wp	PM_{10} exposure				
	Day -1	0.08	-4.51	4.90	0.9729
	Day -2	-0.72	-4.54	3.25	0.7212
	Day -3	-2.92	-6.82	1.13	0.1651
	Day -4	**-5.72**	**-9.48**	**-1.80**	**0.0080**
	Day -5	**-5.77**	**-9.31**	**-2.09**	**0.0047**
	Day -6	**-6.08**	**-9.26**	**-2.78**	**0.0012**
	Day -7	-3.41	-6.86	0.17	0.0709
	$PM_{2.5}$ exposure				
	Day -1	-0.29	-5.37	5.05	0.9134
	Day -2	-0.81	-5.44	4.04	0.7399
	Day -3	-2.41	-6.87	2.25	0.3134
	Day -4	**-5.77**	**-9.74**	**-1.62**	**0.0111**
	Day -5	**-6.42**	**-10.69**	**-1.95**	**0.0090**
	Day -6	**-6.17**	**-10.37**	**-1.77**	**0.0105**
	Day -7	-2.22	-6.91	2.71	0.3782

* Δ% = (exp (β*10) -1) *100, percent increase in DNA methylation for 10 μg/m^3 increase in PM concentration Association between DNA methylation and PM exposure in all subjects. Results from a multivariable regression models adjusted for age, gender, BMI and smoking habit (never, former, current smoker).

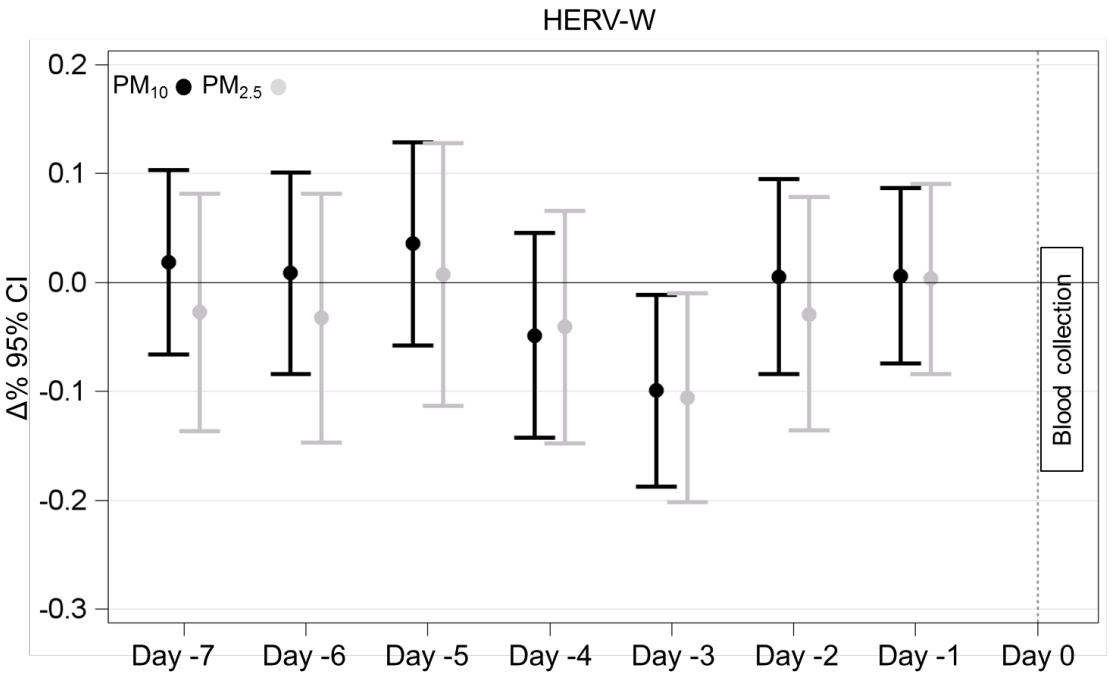

Figure 25. Association between HERV-w methylation and PM_{10} / $PM_{2.5}$ exposures measured at different time lags (from one day before date of blood drawing (Day -1) to Day -7). Linear regression models were adjusted for age, gender, BMI and smoking habit (never, former, current). Δ% = (exp (β*10) -1) * 100 represent the percent increase in HERV-w methylation for 10 μg/m^3 increase in PM concentration

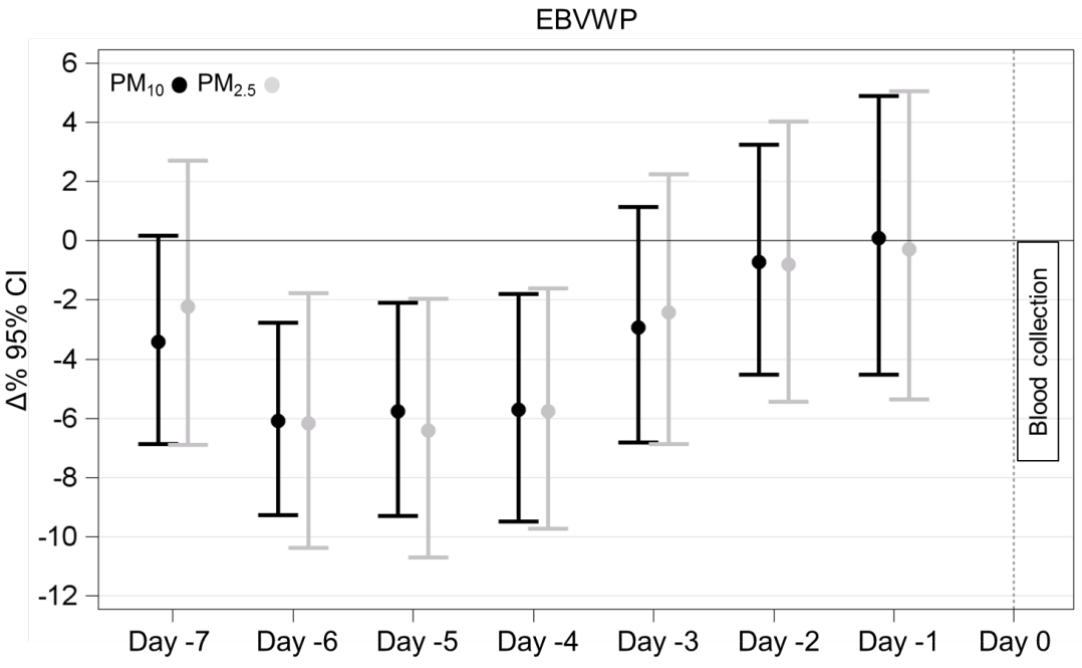

Figure 26. Association of PM_{10} and $PM_{2.5}$ levels measured at different time lags (Day -1 to Day -7) with EBV-Wp methylation. Δ% = (exp (β*10) -1) * 100 represent the percent increase in EBV-Wp methylation for 10 μg/m^3 increase in PM concentration. All models reported were adjusted for age, gender, BMI and smoking habit

SECTION III - EPSTEIN BARR VIRUS REACTIVATION AFTER PM EXPOSURE - IN VITRO STUDY

A purpose of this PhD project was to study Epstain-barr virus cycle in vitro to evaluate a possible association between activation virus status and particulate matter exposure.

This idea arose consequently to a previous study that showed DNA methylation in EBV and HERV-w in a group of healthy steel-workers exposed to particulate matter [111].

This part was done in collaboration with Prof. Paul Farrell at the Imperial College University of London. The main objective of this internship was to study the EBV virology cycle, in order to assess the role of Particulate matter in the EBV reactivation as early protein expression (BZL1) and Wp/Cp methylation.

Five EBV-positive cell lines were investigated: LCL3, GR2, GR104, Mutu I and Akata.

LCL3, GR2 and GR104 are B-lymphoblastoid cell lines (LCLs) in a latency III phase, while Mutu I and Akata cell lines were in a latency I phase. The expression of latency genes which characterize some of these cell lines has been previously reported to be driven from different promoters: Cp for GR-2 and Wp for GR-104 [112], Qp for Akata cells.

WORKFLOW PROCESS

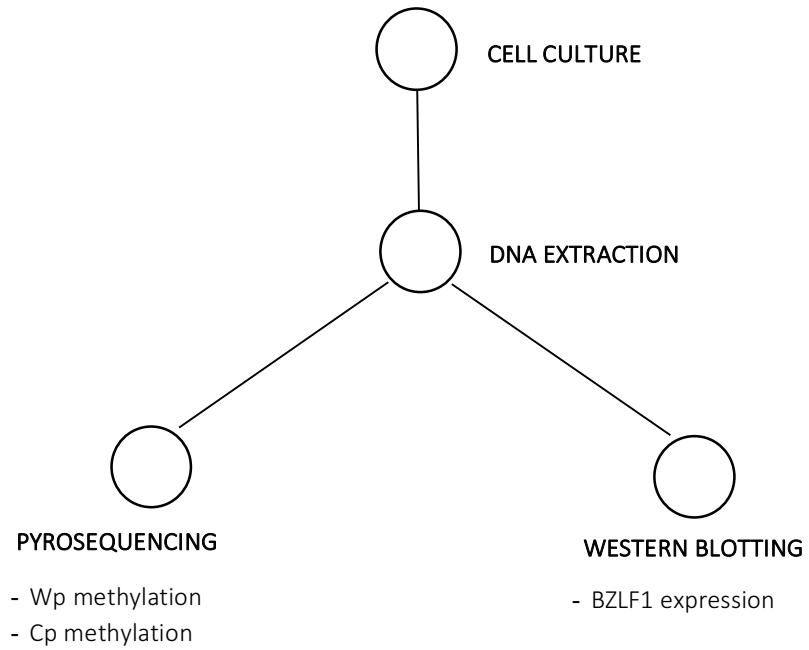

Cell Culture

Cell lines were cultured in RPMI 1640 medium supplemented with 10% fetal bovine serum (FBS) and 0.5% Streptomycin, and grown in a humidified incubator with 5% CO_2 at 37°C. Cells were seeded at a density of 3.0×10^5 cell/ml and treated at 70-80% confluence.

Exposure experiments and DNA extraction in vitro

The exposure experiments were done using Standard Reference Material Urban Particulate Matter (SRM 1648a), an atmospheric particulate matter collected in an urban area intended primarily to be used as a control material.

SRM was suspended in RPMI medium supplemented with 1% FBS and vortex for 30 minutes at room temperature before each exposure experiment.

The cells were exposed for 6-12-24 hours at two different concentrations of particulate matter (10 μg/ml, 62 μg/ml) while, controls cells were incubated with fresh medium alone.

At the end of each experiment, cells were collected and DNA extraction was done using the Wizard Genomic DNA purification kit (Promega, Madison, WI, USA) following the manufacturer's instructions.

Methylation analysis in cell culture

DNA methylation analyses on bisulfite-treated DNA was done using PCR pyrosequencing: 1μg DNA (concentration 50 μg/ μL) was treated using the EZ DNA Methylation-Gold Kit (Zymo Research, Orange, CA, USA) according to the manufacturer's protocol. Final elution was performed with 30 μL M-Elution Buffer.

A 50 μL PCR was turning out in 25 μL GoTaq Green Master mix (Promega), 10 pmol forward primer, 10 pmol reverse primer, 50 ng bisulfite-treated genomic DNA, and water. Primers and PCR cycle conditions are shown in material and method table 4. Reproducibility was increased repeating in duplicate pyrosequencing runs.

Western Blotting

Extracts were prepared by diluting cells into ice-cold PBS, washing twice in ice-cold PBS, and resuspending (4×10^6 cells/100 μl) in a mixture containing ice-cold 50 mM HEPES (pH 7.5), 50 mM NaCl, 0.1% NP-40, 1× protease inhibitor cocktail (Boehringer Mannheim), and 1× phosphatase inhibitor cocktails I and II (Sigma). Cells were then

sonicated briefly on ice and centrifuged for 10 min at 4°C to remove cell debris. Aliquots of the supernatant containing proteins were then snap-frozen and stored at −70°C until further use. Proteins were fractionated by sodium dodecyl sulfate-polyacrylamide gel electrophoresis (SDS-PAGE) and transferred to nitrocellulose membranes.

After incubation for 1 h at room temperature with 5% milk powder made up in PBS-0.1% Tween 20 (PBST), the membranes were probed overnight at 4°C with antibodies. Phosphorylated protein-specific antibodies were diluted and blocked in 2% bovine serum albumin made up in Tris-buffered saline (TBS) -0.1% Tween 20 (TBST). The primary antibody used were anti-BZLF1 (dilution 1:1.000) and anti-GADPH (dilution 1:1.000). After washing with PBST or TBST, membranes were incubated with secondary antibody for 1 h at room temperature. The secondary antibodies used was horseradish peroxidase-conjugated anti-rabbit (Dako) diluted 1:2.000 in 5% milk-PBST. After further washes, bound immunocomplexes were detected by enhanced chemiluminescence (Amersham).

RESULTS

Effects of PM_{10} on cell growth of cell lines with different EBV latency

As a first step, three cell lines characterized by a latency III phase (LCL-3, GR-2 and GR-104) and two by latency I phase (Akata and Mutu-I) were treated with two PM_{10} concentrations (10 μg/ml and 62 μg/ml). After 6, 24 and 48 hours, cell growth was evaluated through hemocytometer, following the manufacture's instruction. Each count was repeated three times and the mean of the three counts recorded. We selected Akata cells to perform the following experiments as their growth were not impacted by PM treatment.

EBV DNA methylation correlates with EBV latency status

The investigation focused the attention on Akata cell lines, treated at two different PM doses (10 μg/ml and 62 μg/ml) for 24 hours.

Methylation analysis confirmed a significant trend of demethylation in treated Akata cell lines as shown in figure 27.

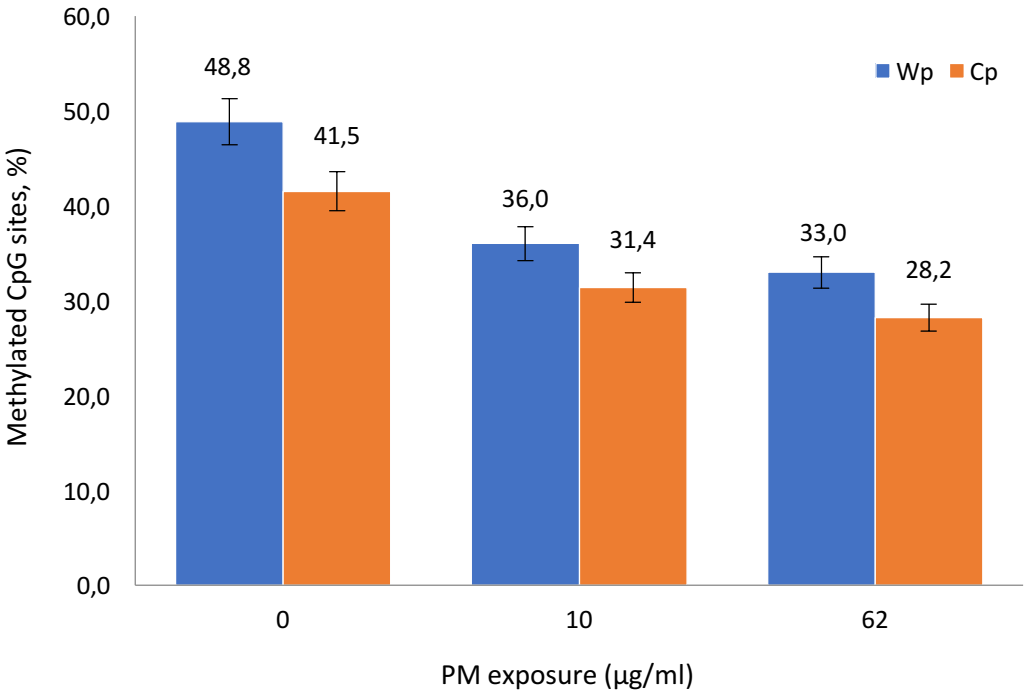

Figure 27. Wp /Cp DNA methylation level cell lines with different viral cycle status, treated with 10 and 62 µg/mL of PM_{10} after 24 hours. Sequence for Wp region (EBV coordinates 1461-14400), and Cp regions (EBV coordinates 11101-11340)

BZLF1- Early Protein expression associated with PM exposure

BZLF1 is the first protein expressed in the reactivation of the EBV lytic cycle [113].

Untreated Akata cells and cells treated with 10 µg/ml or 62 µg/ml PM were incubated for 24 hours at 37° C.

After 24 hours, DNA was extracted and prepared for Western blotting analysis to evaluate BZLF1 expression before and after PM treatment (figure 28).

Western Blotting showed a visible difference in BZLF1 expression between control sample (0 µg/ml) and treated samples, suggesting an induction of this protein by PM.

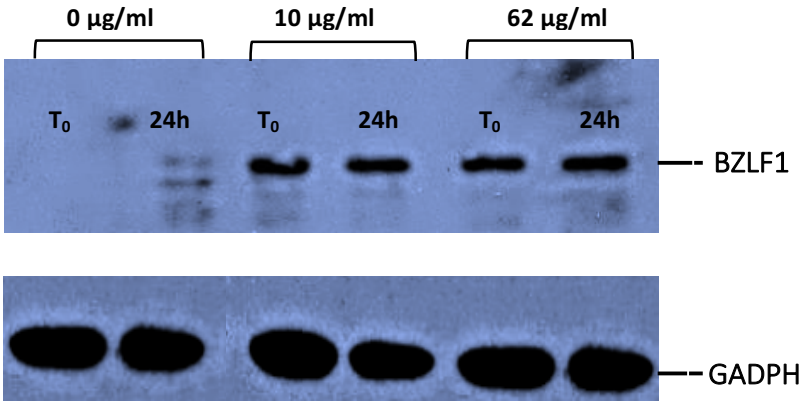

Figure 28. Western Blotting for BZLF1 expression. Akata samples treated with only PM_{10} at two concentrations (10 µ/ml- 62 µ/ml) for 24-h. *BZLF1* size 35-38 kDa; *GADPH* size 36-40 kDa. The concentration for each western blot was 10 µg.

SUMMARY EVALUATION

Akata cell lines showed a reduction in EBV methylation following exposure to PM. This result was consistent with the observed increase in BZLF1, which is the first protein expressed in the reactivation of the EBV lytic cycle.

The reduced methylation in the Akata cells treated with PM_{10} could arise through an active demethylation process, or as unmethylated EBV genomes are produced in the virus replication. Newly replicated EBV DNA and EBV DNA packaged into virus particles is known to be unmethylated. Latently infected Akata cells maintain about 10 episomal copies per cell of the EBV genome but lytic cycle replication can produce up to 500 copies of EBV DNA per cell. Therefore, a small fraction of cells in the lytic cycle could result in a substantial change in the fraction of EBV genomes that is methylated.

A schematic example drawing of this model is illustrated in figure 29.

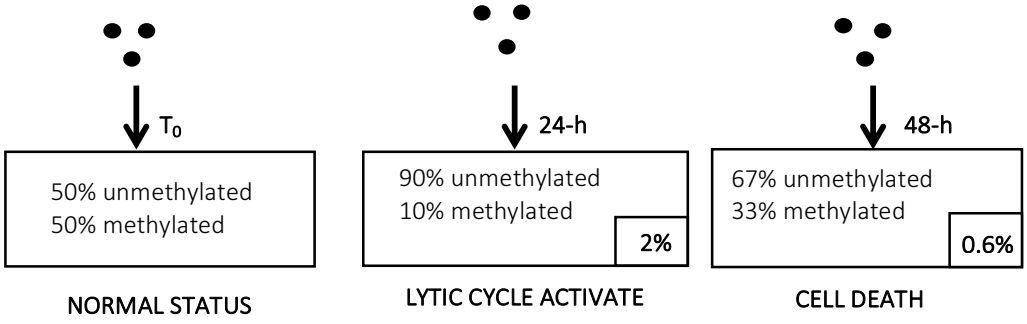

Figure 29. EBV lytic cycle re-activation for Akata cell line treated with PM_{10}. Normal methylation status for time 0 and for my control sample (without PM treated) is 50% methylated and 50% unmethylated. We know that for each cell there are about 10 EBV copies. In this experiment the beginning concentration is $3.0*10^5$ Akata cells in culture, therefore $3*10^6$ EBV copies of which $1.5*10^6$ unmethylated and $1.5*10^6$ methylated. After 24h with 62 μg/ml of PM a little percentage (2%) of EBV infected cell starts the replication and forms a "new unmethylated cells" causing a methylation decrease. 2% of $1.5*10^6$ is $3*10^4$, so $1.5*10^7$ unmethylated cells. The ration between methylated ($1.5*10^6$) and unmethylated ($1.5*10^7$) is ≈10% exactly the value that we obtained in methylation analysis for Akata cell line after 24h. However, after 48h PM starts to become toxic to the cells causing them to die. This event causing the methylation increase and establish new methylation equilibrium

DISCUSSION AND CONCLUSION

Although many epidemiological studies showed an association between PM exposure and diverse health effects, in particular respiratory and cardiovascular diseases, the molecular mechanisms are still largely unknown. A common route might be represented by the systemic activation of pro-inflammatory and pro-oxidant pathways occurring after exposure.

A possible mechanism activated by PM exposure involves the production and modulation of extracellular vesicles, which are powerful carrier of information among cells and tissues. After release, extracellular vesicles (EVs) travel in body fluids (in particular in the bloodstream) and they are able to release their content (e.g. miRNAs, mRNAs, proteins) in other cells, whose gene expression can be modulated by the received signal. A previous study conducted by our research group (Bonzini et al.) on the same study population contributed to support this possible role of EVs in connecting PM exposure to peripheral effects. Short term PM exposure has been, in fact, related to increased EVs concentration in plasma of the investigated subjects. In addition, this study showed how the relationship between PM and EVs was modified by BMI as the effect was much more pronounced in overweight subjects, compared to normal weight subjects.

Another mechanism modulated by environmental factors is DNA methylation [82, 114, 115]. Inhaled particulate pollutants have been shown to determine a status of increased oxidative stress finally producing systemic changes in DNA methylation (e.g. hypomethylation of repetitive elements), which can be detected in peripheral blood of exposed individuals [115]. Repetitive element hypomethylation has been also

associated to viral sequence reactivation [116], suggesting a potential pro-inflammatory mechanism.

In this context, we decided to evaluate various inter-related mechanisms connecting PM exposure to oxidative stress markers (mitochondrial copy number and 8-hydroxydeoxyguanosine) and finally to molecular alterations (viral sequence methylation and telomere length modification).

We followed a two-step approach: an epidemiological study conducted on 50 healthy subjects with a well-characterized exposure to PM_{10} and $PM_{2.5}$ and an in vitro study to confirm the modulation of EBV in cell lines exposed to PM.

Based on evidences from the current literature, showing that variation in epigenetic markers due to environmental stimuli are commonly observed in short time lags, we chose to investigate in the epidemiological study a 1-week lag exposure time window before the day of blood drawing.

In the epidemiological study, we first examined the relationship between short term exposure and two well-known oxidative stress markers: mitochondrial DNA copy number (mtDNA CN) and 8-hydroxydeoxyguanosine (8OHdG). Both PM_{10} and $PM_{2.5}$ exposure were associated to a decreased 8OHdG, in particular at day -3, -5, -6, -7. The effect was mainly determined by overweight subjects. On the contrary, mtDNA CN did not show any significant association with PM exposure. We also evaluated the direct effect of PM exposure on telomere length (TL) and the association between oxidative stress markers and TL. PM exposure was associated to an increased TL, in overweight subjects only. The effect was maximum for day -3 and day -5 both for PM_{10} and $PM_{2.5}$.

Interestingly, both oxidative stress markers showed a negative association with TL again only in overweight subjects.

Apparently our results are in contrast with some literature evidences [117], showing a positive association between PM exposure and oxidative stress markers, such as a negative association between PM exposure and TL.

A possible explanation is given by the fact that all the considered biomarkers are measured only in cells that are still alive, while the cells that are encountering apoptosis following the intense oxidative stress due to PM are no longer available for our analysis. The increased apoptosis would also be a signal for cell renewal, producing a circulating pull of brand new cells, characterized by longer telomeres. In this context, it would be reasonable to think that the more pronounced effect we are observing in overweight subjects is due to the chronic inflammation and oxidative stress that is a standard condition related to high BMI.

When we examined the relationship between oxidative stress markers and TL we found that increased stress markers were related, as expected [118], to a reduction in TL only in overweight subjects. This finding supports the hypothesis that overweight subjects are more susceptible, due to their increased oxidative stress baseline. Adipose tissue produces bioactive molecules (adipokines) which stimulate inflammation and ROS production in leukocytes. For this reason, individuals with an higher BMI might be characterized by an higher baseline of oxidative stress markers, which can influence TL. Moreover, an increased oxidative-stress induced mtDNA damage causes a malfunctioning of the electron transport chain and an increased production of ROS. Free radicals, in turn, cause telomeres to shorten [125].

The second pathway we wanted to study is represented by viral hypomethylation caused by PM exposure. We focused our investigation on the Wp promoter of the Epstein-Barr Virus and the promoter of the human endogenous retrovirus w (HERV-w), respectively as a paradigm of an exogenous virus and an endogenous retroviral sequence.

As expected, we observed an hypomethylation of both HERV-w and EBV in association with PM at Day -3 and Day -4,-5, -6 respectively. This findings is coherent with a previous study we conducted (Mercorio et al.) showing the same effect in 63 male workers of an electric furnace steel plant, exposed to high level of metal-rich particulate matter. The effect of PM on DNA methylation doesn't seem to be modified by BMI of the subjects.

This finding was also confirmed in vitro, as we treated Akata cell lines with PM and we observed an hypomethylation in EBV promoter, such as an increased expression of BZLF1, which is the first protein expressed in the reactivation of the lytic cycle of EBV.

Although our findings are suggestive of a possible mechanism relating PM exposure to molecular outcomes, we recognize some limitations to our study. This is a small-sized study and its results need to be confirmed in a larger independent investigation. Because of the limited number of study subjects, it is possible that the associations observed were due to confounding or chance. The small sample size might have also caused false negative findings. For instance, we did not find any association between mtDNA CN and PM exposure, which was previously reported in several other population.

The cross-sectional design does not allow for investigating the temporal relationship among the different markers we investigated. In fact, we are thinking to the different markers we analyzed as a cascade of events, and indeed the observed effects are related to a different time lags ranging from day -1 to day -6. Unfortunately, for this reason, we could not perform a formal mediation analysis among variables as we could only investigate possible associations between pairs of variables.

The presence of personal air monitoring only for the 24 hours preceding blood drawing, as well as the lack of repeated biological sampling, are also limitations of the study exposure assessment strategy. However, we previously compared PM_{10} and $PM_{2.5}$ levels measured by ambient monitoring stations with those measured through personal samplers at Day -1, and found the two measures to be significantly correlated ($r=0.59$, $P < 0.001$). Furthermore, the two pollutants showed a highly significant inter correlation ($r=0.97$; $P < 0.001$)[103] as expected since $PM_{2.5}$ represents the largest part of PM_{10}

The effect of PM exposure we observed on viral sequence methylation is suggestive of a more global effect affecting all viral sequences in the genome, which might potentially alter systemic inflammation. However, in the present study we limited our analysis to EBV and HERV-w. Future studies are needed to investigate a larger panel of viral sequences, such as to better understand the possible direct effects of virus hypo/hypermethylation on systemic inflammation.

Overall, our investigation provides evidence that short-term exposure to air pollution may impact on 8OHdG, TL and methylation of viral sequences. Our findings, if confirmed in additional investigations, would substantially further our understanding of

molecular mechanisms modified by PM exposure and provide valuable information for the design and timing of blood sample collections for future studies.

REFERENCES

1. (EPA), U.S.E.P.A., *Air Quality Criteria for Particulate Matter.* 2004

2. Siingh, D., et al., *Nucleation events for the formation of charged aerosol particles at a tropical station - Preliminary results.* Atmospheric Research, 2013. **132**: p. 239-252.

3. Curtius, J., *Nucleation of atmospheric aerosol particles.* Comptes Rendus Physique, 2006. **7**(9): p. 1027-1045.

4. Kim, D., M. Gautam, and D. Gera, *Parametric studies on the formation of diesel particulate matter via nucleation and coagulation modes.* Journal of Aerosol Science, 2002. **33**(12): p. 1609-1621.

5. Mishra, K.P., *Lead exposure and its impact on immune system: a review.* Toxicology in Vitro, 2009. **23**(6): p. 969-72.

6. M., G., *Physical and dynamical climatology of the Po Valley.* Regional Meteorological Service 1988.

7. Marcazzan, G.M., et al., *Characterisation of PM10 and PM2.5 particulate matter in the ambient air of Milan (Italy).* Atmospheric Environment, 2001. **35**(27): p. 4639-4650.

8. Kelly, F.J. and J.C. Fussell, *Size, source and chemical composition as determinants of toxicity attributable to ambient particulate matter.* Atmospheric Environment, 2012. **60**: p. 504-526.

9. Michael, S., M. Montag, and W. Dott, *Pro-inflammatory effects and oxidative stress in lung macrophages and epithelial cells induced by ambient particulate matter.* Environ Pollut, 2013. **183**: p. 19-29.

10. Pope, C.A., 3rd, et al., *Lung cancer and cardiovascular disease mortality associated with ambient air pollution and cigarette smoke: shape of the exposure-response relationships.* Environ Health Perspect, 2011. **119**(11): p. 1616-21.

11. Pope, C.A., 3rd, et al., *Cardiovascular mortality and long-term exposure to particulate air pollution: epidemiological evidence of general pathophysiological pathways of disease.* Circulation, 2004. **109**(1): p. 71-7.

12. Klatsky, A.L., *Re: "arsenic exposure and cardiovascular disease: a systematic review of the epidemiologic evidence".* Am J Epidemiol, 2006. **164**(2): p. 194-5; author reply 195-6.

13. Carroll, R.E., *The relationship of cadmium in the air to cardiovascular disease death rates.* JAMA, 1966. **198**(3): p. 267-9.

14. Katsouyanni, K., et al., *Short-term effects of ambient sulphur dioxide and particulate matter on mortality in 12 European cities: results from time series data from the APHEA project. Air Pollution and Health: a European Approach.* BMJ, 1997. **314**(7095): p. 1658-63.

15. Fleisher, J.M. and K. Nayeri, *Re: "Mortality and air pollution in London: a time series analysis".* Am J Epidemiol, 1991. **133**(6): p. 631-3.

16. Longhin, E., et al., *Season linked responses to fine and quasi-ultrafine Milan PM in cultured cells.* Toxicology in Vitro, 2013. **27**(2): p. 551-559.

17. Perrone, M.G., et al., *Seasonal variations in chemical composition and in vitro biological effects of fine PM from Milan.* Chemosphere, 2010. **78**(11): p. 1368-1377.

18. Badyda, A.J., et al., *Exposure to Traffic-Related Air Pollutants as a Risk of Airway Obstruction.* Respiratory Regulation - Clinical Advances, 2013. **755**: p. 35-45.

19. Wang, J., et al., *Contamination characteristics and possible sources of PM10 and PM2.5 in different functional areas of Shanghai, China.* Atmospheric Environment, 2013. **68**: p. 221-229.

20. Boublil, L., et al., *Development of a repeated exposure protocol of human bronchial epithelium in vitro to study the long-term effects of atmospheric particles.* Toxicology in Vitro, 2013. **27**(2): p. 533-542.

21. Li, X.R., et al., *Seasonal variation and source apportionment of organic and inorganic compounds in PM2.5 and PM10 particulates in Beijing, China.* Journal of Environmental Sciences, 2013. **25**(4): p. 741-750.

22. Dergham, M., et al., *Prooxidant and Proinflammatory Potency of Air Pollution Particulate Matter (PM2.5-0.3) Produced in Rural, Urban, or Industrial Surroundings in Human Bronchial Epithelial Cells (BEAS-2B).* Chem Res Toxicol, 2012. **25**(4): p. 904-919.

23. Gualtieri, M., et al., *Airborne urban particles (Milan winter-PM2.5) cause mitotic arrest and cell death: Effects on DNA, mitochondria, AhR binding and spindle organization.* Mutation Research-Fundamental and Molecular Mechanisms of Mutagenesis, 2011. **713**(1-2): p. 18-31.

24. Okuda, T., *Measurement of the specific surface area and particle size distribution of atmospheric aerosol reference materials.* Atmospheric Environment, 2013. **75**: p. 1-5.

25. Reche, C., et al., *A multidisciplinary approach to characterise exposure risk and toxicological effects of PM10 and PM2.5 samples in urban environments.* Ecotoxicol Environ Saf, 2012. **78**: p. 327-335.

26. Schwarze, P.E., et al., *Particulate matter properties and health effects: consistency of epidemiological and toxicological studies.* Hum Exp Toxicol, 2006. **25**(10): p. 559-79.

27. Harris, T.B., et al., *Associations of elevated interleukin-6 and C-reactive protein levels with mortality in the elderly.* Am J Med, 1999. **106**(5): p. 506-12.

28. Pai, J.K., et al., *Inflammatory markers and the risk of coronary heart disease in men and women.* N Engl J Med, 2004. **351**(25): p. 2599-610.

29. Traboulsi, H., et al., *Inhaled Pollutants: The Molecular Scene behind Respiratory and Systemic Diseases Associated with Ultrafine Particulate Matter.* Int J Mol Sci, 2017. **18**(2).

30. Chirino, Y.I., et al., *PM(10) impairs the antioxidant defense system and exacerbates oxidative stress driven cell death.* Toxicol Lett, 2010. **193**(3): p. 209-16.

31. Deng, X., et al., *Airborne fine particulate matter induces multiple cell death pathways in human lung epithelial cells.* Apoptosis, 2014. **19**(7): p. 1099-112.

32. Refsnes, M., et al., *Different particle determinants induce apoptosis and cytokine release in primary alveolar macrophage cultures.* Part Fibre Toxicol, 2006. **3**: p. 10.

33. Aggarwal, B.B., et al., *Inflammation and cancer: how hot is the link?* Biochem Pharmacol, 2006. **72**(11): p. 1605-21.

34. Brant, F., et al., *Role of the aryl hydrocarbon receptor in the immune response profile and development of pathology during Plasmodium berghei Anka infection.* Infect Immun, 2014. **82**(8): p. 3127-40.

35. Alessandri, A.L., et al., *Resolution of inflammation: mechanisms and opportunity for drug development.* Pharmacol Ther, 2013. **139**(2): p. 189-212.

36. Hetland, R.B., et al., *Release of inflammatory cytokines, cell toxicity and apoptosis in epithelial lung cells after exposure to ambient air particles of different size fractions.* Toxicology in Vitro, 2004. **18**(2): p. 203-12.

37. Kaspar, J.W., S.K. Niture, and A.K. Jaiswal, *Nrf2:INrf2 (Keap1) signaling in oxidative stress.* Free Radic Biol Med, 2009. **47**(9): p. 1304-9.

38. Tang, Y., et al., *In vitro cytotoxicity of gold nanorods in A549 cells.* Environ Toxicol Pharmacol, 2015. **39**(2): p. 871-8.

39. Yi, S., et al., *Water-insoluble fraction of airborne particulate matter (PM10) induces oxidative stress in human lung epithelial A549 cells.* Environ Toxicol, 2014. **29**(2): p. 226-33.

40. Avalos, A., et al., *Effects of silver and gold nanoparticles of different sizes in human pulmonary fibroblasts.* Toxicol Mech Methods, 2015. **25**(4): p. 287-95.

41. Periasamy, V.S., et al., *Effects of titanium dioxide nanoparticles isolated from confectionery products on the metabolic stress pathway in human lung fibroblast cells.* Arch Environ Contam Toxicol, 2015. **68**(3): p. 521-33.

42. Montiel-Davalos, A., et al., *TiO(2) nanoparticles induce dysfunction and activation of human endothelial cells.* Chem Res Toxicol, 2012. **25**(4): p. 920-30.

43. Alinovi, R., et al., *Oxidative and pro-inflammatory effects of cobalt and titanium oxide nanoparticles on aortic and venous endothelial cells.* Toxicology in Vitro, 2015. **29**(3): p. 426-37.

44. Petrick, L., et al., *Silicon dioxide nanoparticles increase macrophage atherogenicity: Stimulation of cellular cytotoxicity, oxidative stress, and triglycerides accumulation.* Environ Toxicol, 2016. **31**(6): p. 713-23.

45. Ryter, S.W., et al., *Mechanisms of cell death in oxidative stress.* Antioxid Redox Signal, 2007. **9**(1): p. 49-89.

46. Zhang, X., et al., *Associations of oxidative stress and inflammatory biomarkers with chemically-characterized air pollutant exposures in an elderly cohort.* Environmental Research, 2016. **150**: p. 306-19.

47. Dalton, T.P., H.G. Shertzer, and A. Puga, *Regulation of gene expression by reactive oxygen.* Annu Rev Pharmacol Toxicol, 1999. **39**: p. 67-101.

48. Sambandam, B., et al., *Characterization of coal fly ash nanoparticles and their induced in vitro cellular toxicity and oxidative DNA damage in different cell lines.* Indian J Exp Biol, 2015. **53**(9): p. 585-93.

49. Chan, J.K., et al., *Age-specific effects on rat lung glutathione and antioxidant enzymes after inhaling ultrafine soot.* Am J Respir Cell Mol Biol, 2013. **48**(1): p. 114-24.

50. Cooke, M.S., J. Lunec, and M.D. Evans, *Progress in the analysis of urinary oxidative DNA damage.* Free Radic Biol Med, 2002. **33**(12): p. 1601-14.

51. Kasai, H., *Analysis of a form of oxidative DNA damage, 8-hydroxy-2'-deoxyguanosine, as a marker of cellular oxidative stress during carcinogenesis.* Mutat Res, 1997. **387**(3): p. 147-63.

52. Marczynski, B., et al., *Association between 8-hydroxy-2'-deoxyguanosine levels in DNA of workers highly exposed to asbestos and their clinical data, occupational and non-occupational confounding factors, and cancer.* Mutat Res, 2000. **468**(2): p. 203-12.

53. I.E., S., Mitochondria. Wiley-Liss, New York, NY., 1999.

54. Bogenhagen, D. and D.A. Clayton, *The number of mitochondrial deoxyribonucleic acid genomes in mouse L and human HeLa cells. Quantitative isolation of mitochondrial deoxyribonucleic acid.* J Biol Chem, 1974. **249**(24): p. 7991-5.

55. Nagley, P. and Y.H. Wei, *Ageing and mammalian mitochondrial genetics.* Trends Genet, 1998. **14**(12): p. 513-7.

56. Khrapko, K. and D. Turnbull, *Mitochondrial DNA mutations in aging.* Prog Mol Biol Transl Sci, 2014. **127**: p. 29-62.

57. Hayakawa, M., et al., *Age-related extensive fragmentation of mitochondrial DNA into minicircles.* Biochem Biophys Res Commun, 1996. **226**(2): p. 369-77.

58. Moore, L.D., T. Le, and G. Fan, *DNA methylation and its basic function.* Neuropsychopharmacology, 2013. **38**(1): p. 23-38.

59. Gama-Sosa, M.A., et al., *The 5-methylcytosine content of DNA from human tumors.* Nucleic Acids Res, 1983. **11**(19): p. 6883-94.

60. El-Osta, A., *DNMT cooperativity--the developing links between methylation, chromatin structure and cancer.* Bioessays, 2003. **25**(11): p. 1071-84.

61. Jaenisch, R., *DNA methylation and imprinting: why bother?* Trends Genet, 1997. **13**(8): p. 323-9.

62. Orphanides, G. and D. Reinberg, *A unified theory of gene expression.* Cell, 2002. **108**(4): p. 439-51.

63. Guil, S. and M. Esteller, *DNA methylomes, histone codes and miRNAs: tying it all together.* Int J Biochem Cell Biol, 2009. **41**(1): p. 87-95.

64. Glover, A.B. and B. Leyland-Jones, *Biochemistry of azacitidine: a review.* Cancer Treat Rep, 1987. **71**(10): p. 959-64.

65. Santini, V., H.M. Kantarjian, and J.P. Issa, *Changes in DNA methylation in neoplasia: pathophysiology and therapeutic implications.* Ann Intern Med, 2001. **134**(7): p. 573-86.

66. Kurz, D.J., et al., *Chronic oxidative stress compromises telomere integrity and accelerates the onset of senescence in human endothelial cells.* J Cell Sci, 2004. **117**(11): p. 2417-2426.

67. Feldser, D.M., J.A. Hackett, and C.W. Greider, *Telomere dysfunction and the initiation of genome instability.* Nat Rev Cancer, 2003. **3**(8): p. 623-627.

68. Chan, S.R.W.L. and E.H. Blackburn, *Telomeres and telomerase.* Philosophical Transactions of the Royal Society of London. Series B: Biological Sciences, 2004. **359**(1441): p. 109-122.

69. Harley, C.B., A.B. Futcher, and C.W. Greider, *Telomeres shorten during ageing of human fibroblasts.* Nature, 1990. **345**(6274): p. 458-460.

70. Henle, E.S., et al., *Sequence-specific DNA cleavage by Fe2+-mediated fenton reactions has possible biological implications.* Journal of Biological Chemistry, 1999. **274**(2): p. 962-971.

71. Petersen, S., G. Saretzki, and T.v. Zglinicki, *Preferential Accumulation of Single-Stranded Regions in Telomeres of Human Fibroblasts.* Experimental Cell Research, 1998. **239**(1): p. 152-160.

72. Oikawa, S., S. Tada-Oikawa, and S. Kawanishi, *Site-specific DNA damage at the GGG sequence by UVA involves acceleration of telomere shortening.* Biochemistry, 2001. **40**(15): p. 4763-4768.

73. von Zglinicki, T., *Oxidative stress shortens telomeres.* Trends in Biochemical Sciences, 2002. **27**(7): p. 339-344.

74. Palser, A.L., et al., *Genome diversity of Epstein-Barr virus from multiple tumor types and normal infection.* J Virol, 2015. **89**(10): p. 5222-37.

75. Hadinoto, V., et al., *On the dynamics of acute EBV infection and the pathogenesis of infectious mononucleosis.* Blood, 2008. **111**(3): p. 1420-7.

76. Palser, A.L., et al., *Genome Diversity of Epstein-Barr Virus from Multiple Tumor Types and Normal Infection.* Journal of Virology, 2015. **89**(10): p. 5222-5237.

77. Hutchings, I.A., et al., *Methylation status of the Epstein-Barr virus (EBV) BamHI W latent cycle promoter and promoter activity: analysis with novel EBV-positive Burkitt and lymphoblastoid cell lines.* Journal of Virology, 2006. **80**(21): p. 10700-11.

78. Li, L., et al., *Methylation profiling of Epstein-Barr virus immediate-early gene promoters, BZLF1 and BRLF1 in tumors of epithelial, NK- and B-cell origins.* BMC Cancer, 2012. **12**: p. 125.

79. Niller, H.H., et al., *Epigenetic dysregulation of epstein-barr virus latency and development of autoimmune disease.* Oxygen Transport to Tissue Xxxvi, 2011. **711**: p. 82-102.

80. Ambinder, R.F., K.D. Robertson, and Q. Tao, *DNA methylation and the Epstein-Barr virus.* Semin Cancer Biol, 1999. **9**(5): p. 369-75.

81. Sofer, T., et al., *Exposure to airborne particulate matter is associated with methylation pattern in the asthma pathway.* Epigenomics, 2013. **5**(2): p. 147-54.

82. Baccarelli, A., et al., *Rapid DNA methylation changes after exposure to traffic particles.* Am J Respir Crit Care Med, 2009. **179**(7): p. 572-8.

83. Patel, M.M. and R.L. Miller, *Rapid DNA methylation changes after exposure to traffic particles: the issue of spatio-temporal factors.* Am J Respir Crit Care Med, 2009. **180**(10): p. 1030; author reply 1030-1.

84. Lander, E.S., et al., *Initial sequencing and analysis of the human genome.* Nature, 2001. **409**(6822): p. 860-921.

85. Venter, J.C., et al., *The sequence of the human genome.* Science, 2001. **291**(5507): p. 1304-51.

86. Bollati, V., et al., *Nutrients intake is associated with DNA methylation of candidate inflammatory genes in a population of obese subjects.* Nutrients, 2014. **6**(10): p. 4625-39.

87. Belshaw, R., et al., *High copy number in human endogenous retrovirus families is associated with copying mechanisms in addition to reinfection.* Mol Biol Evol, 2005. **22**(4): p. 814-7.

88. Costas, J., *Characterization of the intragenomic spread of the human endogenous retrovirus family HERV-W.* Mol Biol Evol, 2002. **19**(4): p. 526-33.

89. Pavlicek, A., et al., *Processed pseudogenes of human endogenous retroviruses generated by LINEs: their integration, stability, and distribution.* Genome Res, 2002. **12**(3): p. 391-9.

90. Martin, D. and J.S. Gutkind, *Human tumor-associated viruses and new insights into the molecular mechanisms of cancer.* Oncogene, 2008. **27 Suppl 2**: p. S31-42.

91. McLaughlin-Drubin, M.E. and K. Munger, *Viruses associated with human cancer.* Biochim Biophys Acta, 2008. **1782**(3): p. 127-50.

92. Aftab, A., A.A. Shah, and A.M. Hashmi, *Pathophysiological Role of HERV-W in Schizophrenia.* J Neuropsychiatry Clin Neurosci, 2016. **28**(1): p. 17-25.

93. Morandi, E., et al., *Human endogenous retroviruses and multiple sclerosis: Causation, association, or after-effect?* Mult Scler, 2017. **23**(8): p. 1050-1055.

94. Sutkowski, N., et al., *Epstein-Barr virus transactivates the human endogenous retrovirus HERV-K18 that encodes a superantigen.* Immunity, 2001. **15**(4): p. 579-89.

95. Bergallo, M., et al., *EBV induces HERV-K and HERV-W expression in pediatrics liver transplant recipients?* Minerva Pediatr, 2015.

96. Hristov, M., et al., *Apoptotic bodies from endothelial cells enhance the number and initiate the differentiation of human endothelial progenitor cells in vitro.* Blood, 2004. **104**(9): p. 2761-6.

97. Pisitkun, T., R.F. Shen, and M.A. Knepper, *Identification and proteomic profiling of exosomes in human urine.* Proc Natl Acad Sci U S A, 2004. **101**(36): p. 13368-73.

98. Borges, F.T., et al., *TGF-beta1-containing exosomes from injured epithelial cells activate fibroblasts to initiate tissue regenerative responses and fibrosis.* J Am Soc Nephrol, 2013. **24**(3): p. 385-92.

99. Babst, M., et al., *Endosome-associated complex, ESCRT-II, recruits transport machinery for protein sorting at the multivesicular body.* Dev Cell, 2002. **3**(2): p. 283-289.

100. Wollert, T. and J.H. Hurley, *Molecular mechanism of multivesicular body biogenesis by ESCRT complexes.* Nature, 2010. **464**(7290): p. 864-U73.

101. Raposo, G. and W. Stoorvogel, *Extracellular vesicles: exosomes, microvesicles, and friends.* J Cell Biol, 2013. **200**(4): p. 373-83.

102. Hunter, M.P., et al., *Detection of microRNA expression in human peripheral blood microvesicles.* PLoS One, 2008. **3**(11): p. e3694.

103. Bonzini, M., et al., *Short-term particulate matter exposure induces extracellular vesicle release in overweight subjects.* Environmental Research, 2017. **155**: p. 228-234.

104. Chironi, G., et al., *Circulating leukocyte-derived microparticles predict subclinical atherosclerosis burden in asymptomatic subjects.* Arterioscler Thromb Vasc Biol, 2006. **26**(12): p. 2775-80.

105. Ueba, T., et al., *Plasma level of platelet-derived microparticles is associated with coronary heart disease risk score in healthy men.* J Atheroscler Thromb, 2010. **17**(4): p. 342-9.

106. Loyer, X., et al., *Microvesicles as cell-cell messengers in cardiovascular diseases.* Circ Res, 2014. **114**(2): p. 345-53.

107. Pergoli, L., et al., *Extracellular vesicle-packaged miRNA release after short-term exposure to particulate matter is associated with increased coagulation.* Part Fibre Toxicol, 2017. **14**(1): p. 32.

108. *The use of ICP-MS for human biomonitoring.* Bimonitoring methods **6**.

109. Carugno, M., et al., *Air pollution exposure, cause-specific deaths and hospitalizations in a highly polluted Italian region.* Environ Res, 2016. **147**: p. 415-24.

110. Houben, J.M.J., et al., *Telomere length assessment: Biomarker of chronic oxidative stress?* Free Radical Biology and Medicine, 2008. **44**(3): p. 235-246.

111. Mercorio, R., et al., *Effects of metal-rich particulate matter exposure on exogenous and endogenous viral sequence methylation in healthy steel-workers.* Environmental Research, 2017. **159**: p. 452-457.

112. Evans, T.J., P.J. Farrell, and S. Swaminathan, *Molecular genetic analysis of Epstein-Barr virus Cp promoter function.* J Virol, 1996. **70**(3): p. 1695-705.

113. Amon, W., et al., *Lytic cycle gene regulation of Epstein-Barr virus.* J Virol, 2004. **78**(24): p. 13460-9.

114. Baccarelli, A. and V. Bollati, *Epigenetics and environmental chemicals.* Curr Opin Pediatr, 2009. **21**(2): p. 243-51.

115. Tarantini, L., et al., *Effects of particulate matter on genomic DNA methylation content and iNOS promoter methylation.* Environ Health Perspect, 2009. **117**(2): p. 217-22.

116. Rebollo, R., M.T. Romanish, and D.L. Mager, *Transposable elements: an abundant and natural source of regulatory sequences for host genes.* Annu Rev Genet, 2012. **46**: p. 21-42.

117. Hoxha, M., et al., *Association between leukocyte telomere shortening and exposure to traffic pollution: a cross-sectional study on traffic officers and indoor office workers.* Environ Health, 2009. **8**: p. 41.

118. Oikawa, S. and S. Kawanishi, *Site-specific DNA damage at GGG sequence by oxidative stress may accelerate telomere shortening.* FEBS Lett, 1999. **453**(3): p. 365-8.